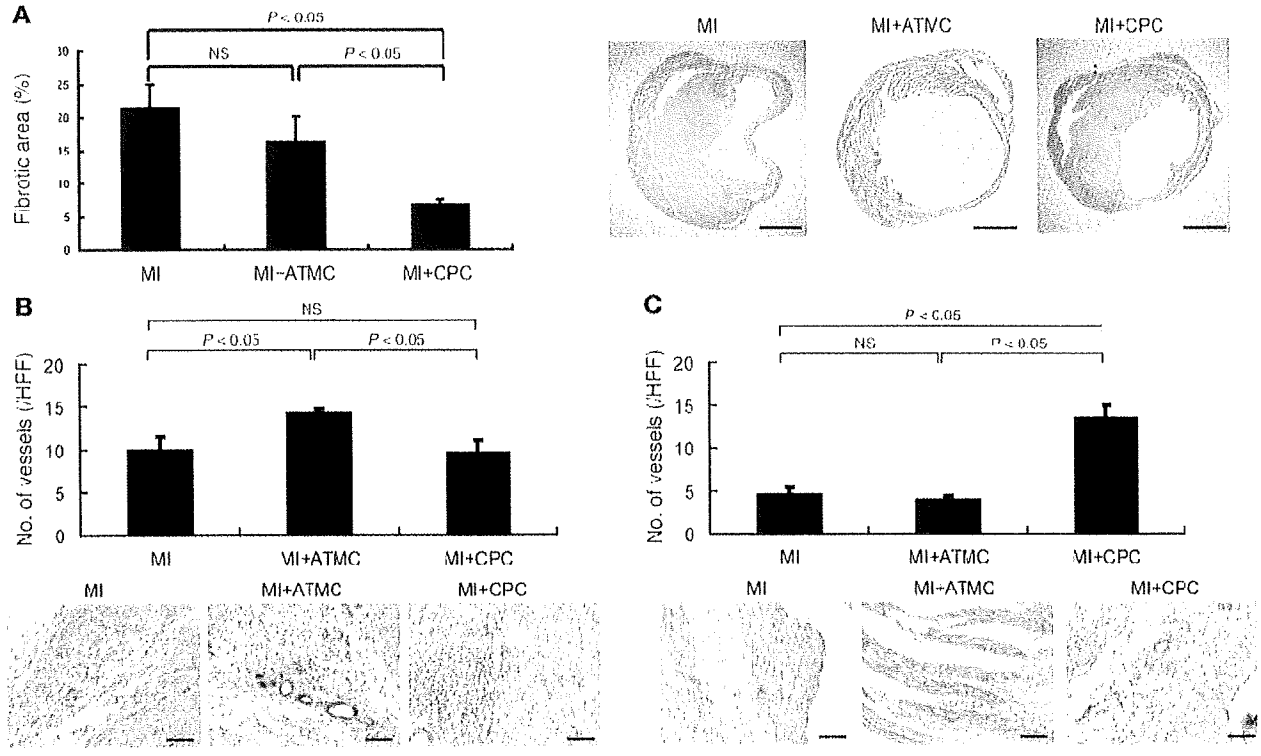

Figure 3

Immunohistochemical analysis of transplanted hearts. (**A**) Masson trichrome staining. The fibrotic area at 4 weeks after transplantation was calculated and is shown in the graph (n = 6). Lower panels show representative images. Scale bars: 1 mm. (**B** and **C**) Endothelial cells were identified by immunohistochemical staining with anti-vWF Ab in the border zone of the infarcted hearts 1 week (**B**) and 4 weeks (**C**) after transplantation. Lower panels show representative images. The vessel number was quantified and is depicted in the graph (n = 6). HPF, high-power field. Scale bars: 100 μm. Data are shown as mean + SEM.

effects of CPC-derived CM and sVCAM-1 on cardiomyocytes were analyzed. When cardiomyocytes were pretreated with CPC-derived CM or sVCAM-1, H_2O_2-induced damage of cardiomyocytes was significantly reduced (Figure 6A). The cardioprotective effects of CPC-derived CM were abolished by pretreatment of cardiomyocytes with Abs against very late antigen-4 (VLA-4, also known as $\alpha_4\beta_1$ integrin), a principal coreceptor of sVCAM-1 (Figure 6A), or sVCAM-1–depleted CM (Figure 6B). These results suggested a crucial role for sVCAM-1/VLA-4 in cardiomyocyte survival.

Integrin-mediated signals influence cardioprotective effects of sVCAM-1. Integrin-mediated signaling induces cell migration and survival by activating various kinases, such as focal adhesion kinase (FAK), Akt, ERK1/2, and p38 MAPK (21, 22). CPC-derived CM and sVCAM-1 induced phosphorylation and activation of FAK, Akt, ERK, and p38 MAPK in neonatal rat cardiomyocytes (Figure 6, C and E). When cardiomyocytes were pretreated with inhibitors of Akt, PI3K (wortmannin), p38 MAPK (SB203580), or ERK (PD98059), the cardioprotective effects of CPC-derived CM and sVCAM-1 were significantly inhibited (Figure 6, D and F). When cardiomyocytes were pretreated with anti–VLA-4 Abs prior to culturing in CPC-derived CM, phosphorylation of FAK, Akt, and ERK but not p38 MAPK was inhibited (Figure 6E). This suggests that the protective effects of CPC-derived CM on cardiomyocytes were achieved through sVCAM-1/VLA-4–mediated activation of Akt and ERK as well as VLA-4–independent activation of p38 MAPK.

sVCAM-1–induced migration of CPCs. Because a large number of transplanted CPCs migrated from the epicardial cell sheet to the ventricular myocardium following transplantation (Figure 4A), the effects of CPC-derived CM and sVCAM-1 on CPC migration were analyzed. When treated with CPC-derived CM or sVCAM-1, CPC migration was promoted, and anti–VLA-4 Abs or sVCAM-1 depletion markedly inhibited CM-induced migration of CPCs (Figure 6G). When CPCs were treated with sVCAM-1, phospho–p38 MAPK expression was significantly increased. However, expression of phospho-Akt and phospho-ERK remained unchanged. Phosphorylation of p38 MAPK was significantly inhibited by anti–VLA-4 Ab treatment (Figure 6H), which suggested that CPCs activated p38 MAPK through VLA-4. SB203580 inhibited CPC-derived CM- and sVCAM-1–induced CPC migration compared with the control (Figure 6I). These findings suggest that CPCs secreted sVCAM-1 and induced CPC migration via the VLA-4/p38 MAPK signaling pathway. Moreover, when VCAM-1 expression was downregulated, CPC viability was significantly decreased and apoptosis increased (Supplemental Figure 10), suggesting that VCAM-1 might be important for CPC survival.

VLA-4 signaling plays a crucial role in the beneficial effects of CPC sheet transplantation. The present findings suggest that CPC-secreted sVCAM-1 induced angiogenesis as well as CPC migration and survival and protected cardiomyocytes via VLA-4 in vitro. Subsequently, VLA-4 signaling was analyzed to determine its role in improved

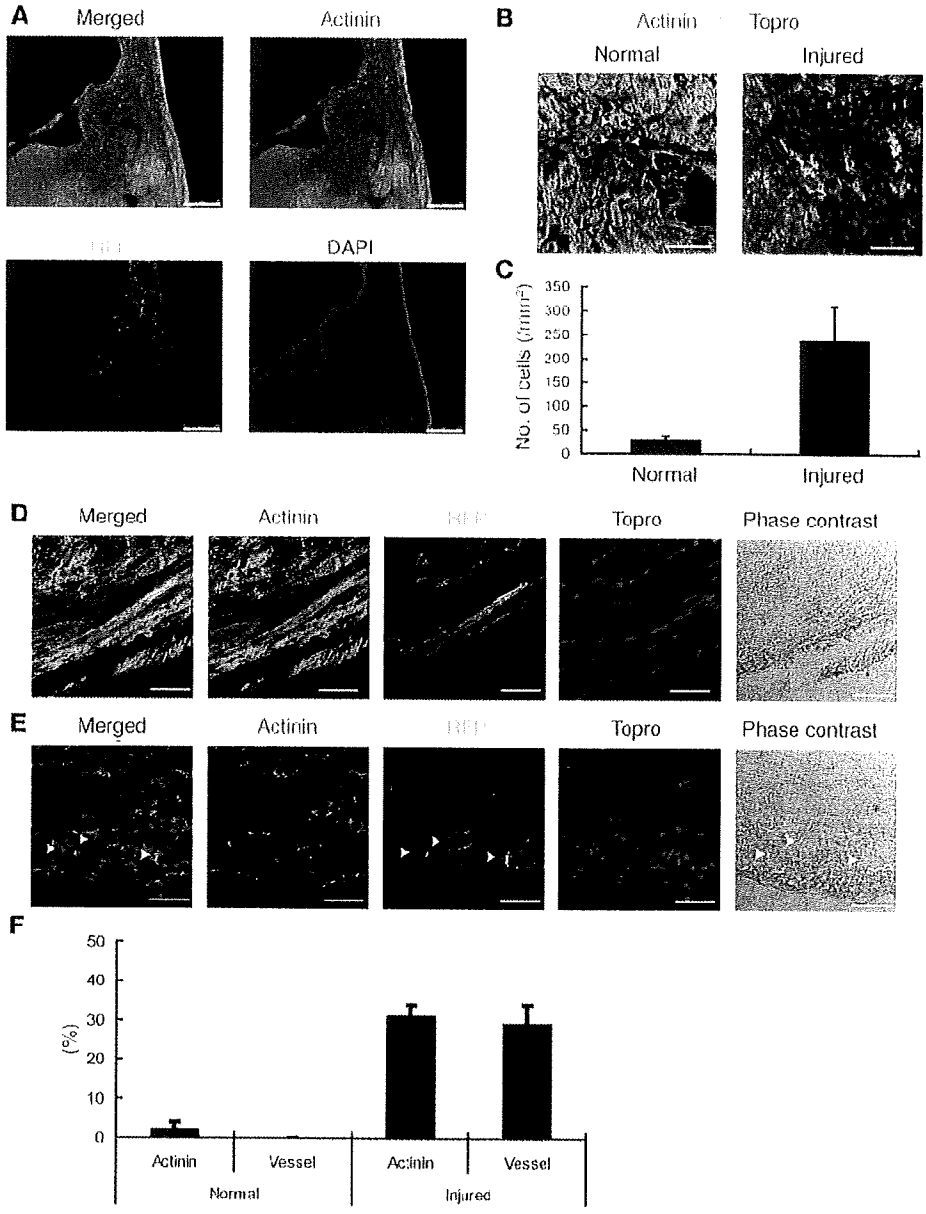

Figure 4
Cell survival and differentiation of transplanted cells. (**A**) Fluorescent microscopic images of infarcted heart 4 weeks after RFP$^+$ CPC sheet transplantation. Left sides of panels show endocardial area. Right sides of panels show epicardial area. Scale bars: 250 μm. (**B**) Confocal microscopic images of infarcted heart 4 weeks after CPC sheet transplantation (sarcomeric α-actinin, green; RFP, red; Topro, blue; yellow in merged images). Left panel shows normal area. Right panel shows injured area. Arrowheads indicate RFP$^+$ cells. Scale bars: 5 μm. (**C**) Number of RFP$^+$ cells were quantified and shown in the graph (n = 5). (**D** and **E**) Transplanted RFP$^+$ cells expressed sarcomeric α-actinin in a fine striated pattern (**D**) and formed vessel structures around α-actinin–positive myocardium (**E**). Nuclei were stained with Topro. Arrowheads indicate vessel structures. Scale bars: 5 μm. (**F**) Percentages of α-actinin–positive cells or vessel structure–forming cells in existing RFP$^+$ cells were calculated and shown in the graph (n = 5). Data are shown as mean + SEM.

cardiac function following transplantation of CPC sheets. Because echocardiographic analysis revealed improved cardiac function 3 weeks after transplantation (Figure 2A), i.p. injection of anti–VLA-4 Abs was performed daily from 2 to 3 weeks after CPC sheet transplantation. At 4 weeks after transplantation, injection of anti–VLA-4 Abs significantly attenuated the beneficial effects of CPC sheet transplantation on cardiac function, fibrosis, and angiogenesis (Figure 7, A–D). The number of RFP$^+$ CPCs in the infarcted area was also markedly decreased following treatment with anti–VLA-4 Abs (Figure 7E). In contrast, anti–VLA-4 Ab treatment did not affect cardiac function, fibrotic area, or blood vessel number in nontransplanted MI mice (Supplemental Figure 11). These findings suggest that CPC sheet transplantation improved cardiac function of infarcted hearts through VLA-4–mediated angiogenesis as well as survival and migration of transplanted CPCs.

Discussion

The present study reports that CPC sheet transplantation inhibited cardiac remodeling and restored cardiac function after MI by increasing the number of blood vessels and cardiomyocytes in the injured area. sVCAM-1 was identified as one of the dominant paracrine factors in CPCs and was shown to induce angiogenesis, cardioprotection, and CPC migration and survival through the VLA-4 signaling pathway. Therefore, sVCAM-1 plays a critical role in improved cardiac function following MI.

CPC transplantation restored cardiac function and angiogenic activity and prevented cardiac remodeling 4 weeks after transplantation. In contrast, ATMC transplantation attenuated cardiac dysfunction and enhanced angiogenesis transiently, and cardiac remodeling progressed at 4 weeks. These findings suggest varying cell survival rates (Supplemental Figure 3) and

Table 2
Results of cytokine Ab array

Cytokine	Fold increase
CPC	
VCAM-1	130.1
MIP-1γ	23.4
TIMP-1	8.0
IL-6	7.0
GM-CSF	6.0
IL-17	5.8
IL-5	5.3
KC	5.2
IFN-γ	5.2
IL-10	5.2
IL-12 p40/p70	4.8
IL-4	4.6
SDF-1α	4.5
IL-2	4.5
IL-12 p70	4.0
TNFα	3.9
MIP-3β	3.8
MIG	3.6
IL-9	3.1
MCP1	3.1
Osteopontin	2.1
ATMC	
MIP-1γ	135.7
KC	43.6
VCAM-1	22.4
RANTES	13.6
TIMP-1	11.9
IL-6	9.8
LIX	6.3
CXCL16	6.1
IL-17	5.6
GM-CSF	5.4
IL-2	4.8
IL-5	4.8
IL-4	4.3
IL-12 p70	4.2
IFN-γ	3.8
IL-10	3.6
IL-12 p40/p70	3.5
IL-9	3.4
Eotaxin	3.4
VEGF	3.2
TNFα	2.9
MCP1	2.9
MIP-3β	2.8
Osteopontin	2.5
MIG	2.4
CRG-2	2.2
SDF-1α	2.1

Each number indicates the fold increase of cytokine expression compared with the negative control. Serum-depleted medium was used as a negative control. SDF-1α, stromal cell–derived factor-1α; MIP-1γ, macrophage inflammatory protein-1γ; KC, keratinocyte-derived chemokine; TIMP-1 tissue inhibitor of metalloproteinase 1; LIX, LPS-induced chemokine; MCP1, monocyte chemotactic protein-1; MIG, monokine induced by gamma; CRT-2, cytokine-responsive gene-2.

distinct protein expression profiles (Figure 5B) in CPCs and ATMCs in the transplanted areas.

Through direct comparison of the protein expression profiles of CPCs and ATMCs, sVCAM-1 was identified as one of the predominantly expressed CPC-derived paracrine factors. VCAM-1, a 110-kDa transmembrane glycoprotein, is detected in various cells, including endothelial and bone marrow stromal cells (23). A soluble form of VCAM-1 has been reported to be shed from VCAM-1 on the cell surface by proteases, including TNF-α–converting enzyme (24). TNF-α–converting enzyme has also been reported to be elevated in the myocardium in heart failure (25) and to be required for fetal murine cardiac development and modeling (26). sVCAM-1 induces migration of endothelial cells through VLA-4 (21, 27, 28). The present study demonstrates that CM from VCAM-1–knocked-down CPCs did not induce endothelial migration, tube formation, cardioprotection, or CPC migration. Anti–VLA-4 Ab treatment abolished the protective effects of CPC-derived CM on cardiomyocytes and migration of CPCs and attenuated improved cardiac function following CPC sheet transplantation. This suggests that sVCAM-1 is a major paracrine factor of cardioprotection. VLA-4 is an integrin dimer that is composed of CD49d (α_4) and CD29 (β_1). Although studies have shown that the β_1 integrin signaling cascade regulates migration, differentiation, and death of various types of cells, such as endothelial cells, cardiomyocytes, and epidermal and hematopoietic stem cells (29–31), the role of sVCAM-1–mediated VLA-4 signaling in stem/progenitor cells remains elusive.

CPC-derived CM and sVCAM-1 phosphorylated several integrin-related downstream signaling molecules, such as Akt, ERK, and p38 MAPK, in cardiomyocytes. Consistent with previous studies, which indicated that Akt and ERK are critical for growth and survival of cardiomyocytes (32, 33), this study showed that promotion of cardiomyocyte survival by CPC-derived CM and sVCAM-1 was regulated through VLA-4–mediated activation of Akt and ERK. Furthermore, migration of CPCs, almost all of which expressed CD29 (β_1 integrin; Supplemental Figure 1), was facilitated via the VLA-4/p38 MAPK signaling pathway. VCAM-1–knockout mice and α_4 integrin–null mice have been shown to exhibit embryonic lethality, which was partly attributed to impaired epicardium formation surrounding the ventricular and atrial chambers, which suggests that VCAM-1/α_4 integrin signaling is critical for heart development (34, 35). In the present study, anti–VLA-4 Ab treatment reduced survival of transplanted CPCs. Furthermore, when VCAM-1 of CPCs was downregulated by specific miRNA, CPC viability was reduced and apoptosis was increased (Supplemental Figure 10), which suggests that VCAM-1–mediated signaling is also important for CPC survival. Since transplanted CPCs are the sources of not only paracrine factors but also newly formed cardiomyocytes, VCAM-1–mediated paracrine effects might also contribute to the cardiomyogenesis of CPCs through improved engraftment. A recent study has suggested that adult cardiac stem cells express α_4 and β_1 integrin in the niches (36). However, the role of α_4 and β_1 integrins is not fully understood. Since adult mammalian cardiomyocytes have been reported to be refreshed by endogenous stem cells after injury (37), our results suggest that sVCAM-1 secreted from transplanted CPCs promoted migration and self renewal of not only transplanted CPCs, but also endogenous cardiac stem/progenitor cells, through α_4 and β_1 integrin.

VCAM-1 is known as an inflammatory mediator, and increased sVCAM-1 in plasma has been reported following acute MI (38). During acute-phase MI, infiltrating leukocytes release cytokines,

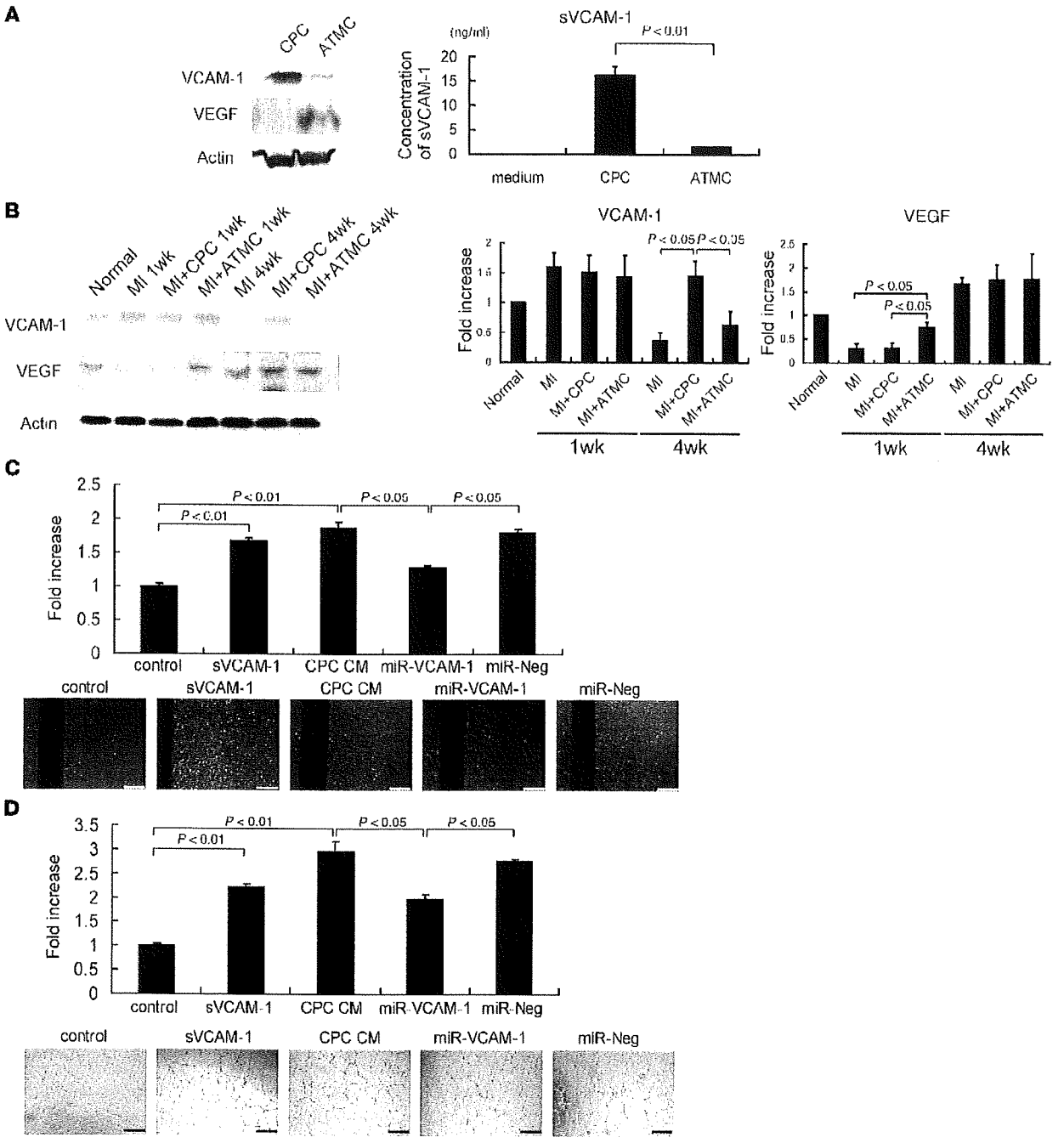

Figure 5

Secreted factor–mediated angiogenesis. (**A**) Left panel shows Western blot analysis results using whole-cell lysates of cultured CPCs and ATMCs. Right panel shows the results of sVCAM-1 ELISA using CM from cultured CPCs and ATMCs (n = 3). (**B**) Western blot analysis results of VCAM-1 and VEGF expression in heart after MI. Normal heart was used as a control. Left panel shows representative images. Right panels show quantification results of VCAM-1 and VEGF expression (n = 3). (**C**) Scratch-wound assay. CPC-derived CM enhanced endothelial migration (n = 3). Lower panels show representative images (n = 3). Scale bars: 500 μm. (**D**) CPC-derived CM enhanced endothelial tube formation. Tube length was quantified and is shown in the graph (n = 3). Lower panels show representative images. Scale bars: 500 μm. miR, miRNA. Data are shown as mean + SEM.

which activate VCAM-1 expression and promote leukocyte transmigration. In the present study, increased VCAM-1 expression in myocardium was observed in each group 1 week after MI/transplantation, when many inflammatory cells were also observed (data not shown). At 4 weeks, however, VCAM-1 expression remained upregulated in the CPC group despite few inflammatory

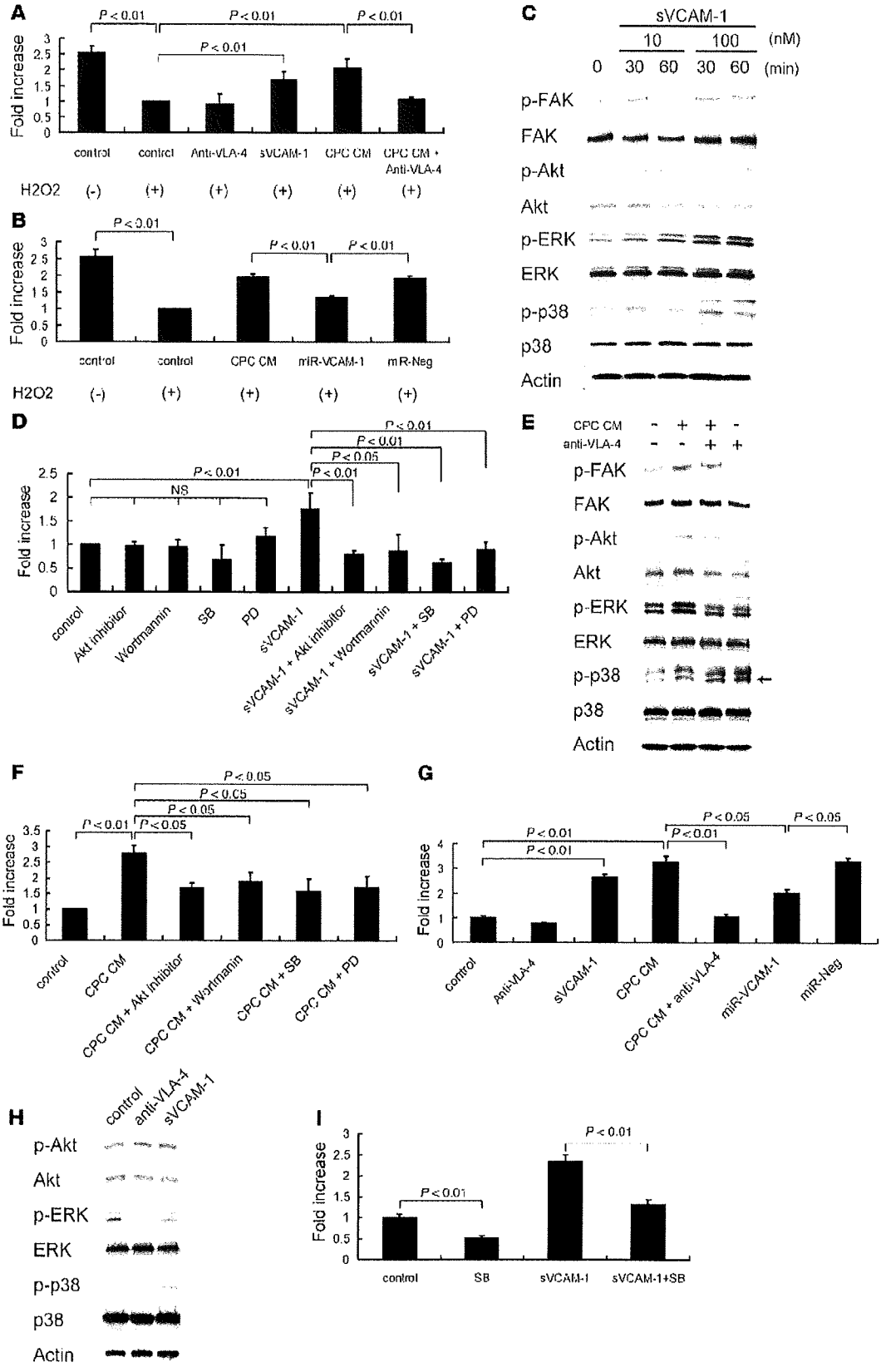
A
Fold increase
control
control
Anti-VLA-4
sVCAM-1
CPC CM
CPC CM + Anti-VLA-4
H2O2
B
control
control
CPC CM
miR-VCAM-1
miR-Neg
C
sVCAM-1
10
100
(nM)
0 30 60 30 60 (min)
p-FAK
FAK
p-Akt
Akt
p-ERK
ERK
p-p38
p38
Actin
D
NS
control
Akt inhibitor
Wortmannin
SB
PD
sVCAM-1
sVCAM-1 + Akt inhibitor
sVCAM-1 + Wortmannin
sVCAM-1 + SB
sVCAM-1 + PD
E
CPC CM
anti-VLA-4
F
control
CPC CM
CPC CM + Akt inhibitor
CPC CM + Wortmannin
CPC CM + SB
CPC CM + PD
G
control
Anti-VLA-4
sVCAM-1
CPC CM
CPC CM + anti-VLA-4
miR-VCAM-1
miR-Neg
H
control
anti-VLA-4
sVCAM-1
p-Akt
Akt
p-ERK
ERK
p-p38
p38
Actin
I
control
SB
sVCAM-1
sVCAM-1+SB

Figure 6
sVCAM-1–mediated cardioprotective effects and CPC migration. (**A** and **B**) Cardiomyocyte viability following treatment with H_2O_2 was measured by MTT assay ($n = 3$). IgG isotype Abs were used as a control (**A**). (**C**) sVCAM-1 induced phosphorylation of FAK, Akt, ERK, and p38 MAPK in a dose-dependent manner. (**D**) Cardiomyocyte viability following treatment with H_2O_2 was measured by MTT assay ($n = 4$). SB, SB2035800; PD, PD98059. (**E**) CPC-derived CM induced phosphorylation of FAK, Akt, ERK, and p38 MAPK. Anti–VLA-4 Abs inhibited phosphorylation of FAK, Akt, and ERK induced by CPC-derived CM, but not phosphorylation of p38 MAPK. Arrow indicates appropriate size of phosphorylated p38 MAPK. (**F**) Cardiomyocyte viability following treatment with H_2O_2 was measured by MTT assay ($n = 4$). (**G** and **I**) CPC migration was measured using the scratch wound assay ($n = 3$). IgG isotype Ab was used as a control (**G**). (**H**) Anti–VLA-4 Abs inhibited phosphorylation of ERK and p38 MAPK of CPCs, but not Akt. Activity of p38 MAPK, but not Akt or ERK, was upregulated by sVCAM-1 treatment. Data are shown as mean + SEM.

cells in the infarcted area (Supplemental Figure 5). Furthermore, peripheral blood concentrations of sVCAM-1 were similar between groups 1 and 4 weeks after transplantation, which suggested that VCAM-1 expression in the transplanted heart was derived from CPC sheets, rather than circulating cells in the peripheral blood. VCAM-1 and its receptor, VLA-4, are important for fusion between hematopoietic progenitor cells and cardiomyocytes (39), and Oh et al. have reported that approximately 50% of cardiac protein–expressing transplanted cells arise from fusion with existing cardiomyocytes (3), which suggests that VCAM-1 mediates fusion between CPCs and dormant cardiomyocytes.

The present study compared transplanted cell survival between cell sheet transplantation and direct cell injection (Supplemental Figures 2 and 3). At 1 week after cell sheet transplantation, approximately 40% of cells survived (Supplemental Figure 3), while only 10% of cells survived after direct cell injection (Supplemental Figure 2). Immediately following transplantation, RFP expression in the heart was similar between cell sheet transplantation and direct cell injection, which suggested that the initial transplantation efficiency was the same. These findings indicate that cell sheet transplantation was superior to direct injection into the myocardium.

Many reports have demonstrated that endogenous cardiac stem/progenitor cells or bone marrow–derived cells mobilize to the infarcted area after injury and recruit additional cells through a feedback mechanism (40, 41). As shown in Table 2, CPCs expressed several chemokines, including stromal cell–derived factor-1 (SDF-1), which recruits bone marrow–derived cells to the infarcted myocardium (42). Therefore, CPC sheet transplantation may induce migration of bone marrow–derived cells to the infarcted heart, thereby improving cardiac function. Recently, anti-α_4 integrin Ab treatment was shown to improve cardiac function 2 weeks after MI by inhibiting interactions between bone marrow cells and their niches and promoting bone marrow cell migration and vasculogenesis (43). In the present study, anti–VLA-4 Ab treatment significantly attenuated improved cardiac function and angiogenesis following CPC sheet transplantation. Moreover, anti–VLA-4 Ab treatment did not affect cardiac function, fibrotic area, or blood vessel number in nontransplanted MI mice (Supplemental Figure 11). These findings suggest that bone marrow cells from their niches do not significantly contribute to the beneficial effects of CPC sheet transplantation.

There were a few limitations to the present study. The CPCs used in the experiments exhibited gene expression patterns similar to those of freshly isolated cardiac Sca-1–positive cells. However, profiles associated with proliferation, migration, and cardiomyocyte differentiation may not be the same. HUVECs were employed in endothelial migration and tube formation assays in vitro, and there might be differences between HUVECs and cardiac endothelial cells. Nevertheless, CPC sheet-mediated transplantation might be superior to the combination of other cell sources and tissue engineering methods. Improved survival of transplanted CPCs, in combination with several growth factors (44, 45), or multilayered cell sheets (46) might improve the beneficial effects of CPC sheet transplantation.

The present study identified the VCAM-1/VLA-4 signaling pathway as an important mechanism for CPC transplantation–mediated improved cardiac function. However, other paracrine factors, including thymosin β4 (47), have also been reported to contribute to cardiac repair following MI. Therefore, multiple mechanisms and mutual crosstalk might be involved in cell sheet transplantation to improve cardiac function. It remains to be determined which mechanisms are the most important and should be improved.

Methods

Animals. Wild-type mice (C57BL/6J) were purchased from Japan SLC. Adult GFP transgenic mice (C57BL/6J) were a gift from Masaru Okabe, Osaka University (Osaka, Japan). Neonatal Wistar rats (0 to 1 day old) were purchased from Saitama Experimental Animals Supply. All protocols were approved by the Institutional Animal Care and Use Committee of Tokyo Women's Medical University and Chiba University.

Reagents. FITC-conjugated anti-CD29, PE-conjugated anti–Sca-1, anti-CD44, and anti–c-kit Abs were purchased from eBioscience. PE-conjugated anti-CD31, anti-CD34, and anti-CD45 Abs were purchased from BD Biosciences – Pharmingen. The following Abs were used for immunostaining and Western blot analysis: mouse monoclonal anti-sarcomeric α-actinin, mouse monoclonal anti-β-actin (Sigma-Aldrich), rat monoclonal anti–VLA-4, mouse monoclonal anti–β-myosin heavy chain (anti–β-MHC) (Chemicon; Millipore), goat polyclonal anti-Nkx2.5, goat polyclonal anti-GATA4, rabbit polyclonal anti–atrial natriuretic peptide (anti-ANP), rabbit polyclonal anti-VEGF, goat polyclonal anti-Akt, rabbit polyclonal anti-FAK (Santa Cruz Biotechnology Inc.), rabbit polyclonal anti-GFP, rabbit polyclonal anti-RFP (MBL International Corp.), rabbit polyclonal anti–VCAM-1 (R&D Systems), rabbit polyclonal anti-vWF (Dako), rabbit polyclonal anti–myocyte enhancer factor 2C (anti-MEF2C), rabbit polyclonal anti-phospho Akt (Ser473), rabbit polyclonal anti-phospho p38 MAPK (Thr180/Tyr182), rabbit polyclonal anti-p38 MAPK, rabbit polyclonal anti-phospho ERK1/2, rabbit polyclonal anti-ERK 1/2 (Cell Signaling Technology), and rabbit monoclonal anti-phospho FAK (Y397; Invitrogen). Secondary Abs were purchased from Jackson ImmunoResearch Laboratories Inc. Unless otherwise specified, reagents were purchased from Sigma-Aldrich.

Cell isolation. Sca-1–positive cells were isolated from an adult (10 weeks old) wild-type, male mouse, as described previously (4). Isolated cells (1×10^4) were harvested on a 10-cm Primaria dish (BD Falcon) in Iscove's Modified Dulbecco's Medium (IMDM) (Invitrogen) supplemented with 10% FBS and penicillin/streptomycin at 37°C in humid air with 5% CO_2. One month after starting culture, several colonies were recognizable. Each of these colonies was collected using a cloning cup and reseeding to a new 10-cm Primaria dish. After repeating this process 2 more times, a clonal cell line was established.

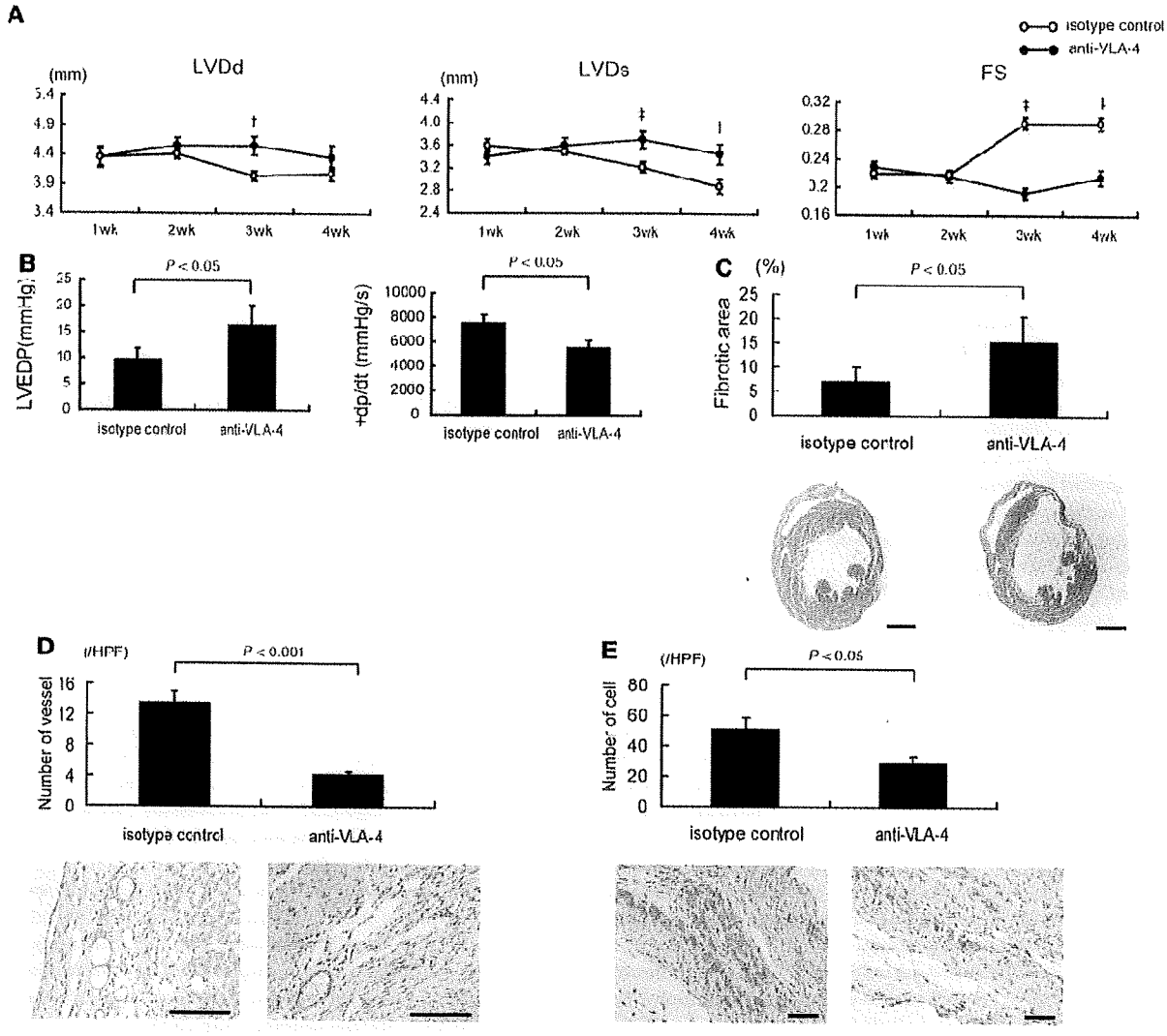

Figure 7

The roles of VLA-4 signaling on CPC sheet transplantation-mediated improved cardiac function. Analysis of cardiac function by echocardiography (**A**, $n = 5$) and catheterization (**B**, $n = 5$). Anti–VLA-4 Ab treatment inhibited the reduction of LVDd, LVDs, and LVEDP and the improvement of FS and +dp/dt by CPC sheet transplantation. Isotype Ab was used as a control. †$P < 0.05$ versus anti–VLA-4 Abs ($n = 5$ per group). ‡$P < 0.01$ versus anti–VLA-4 Abs ($n = 5$ per group). (**C**) Masson trichrome staining. The fibrotic area 4 weeks after transplantation was calculated and is shown in the graph ($n = 5$). Anti–VLA-4 Ab treatment inhibited the reduction of fibrotic area following CPC sheet transplantation. Lower panels show representative images. Scale bars: 1 mm. (**D**) vWF staining. The number of vWF-positive vessels in the border area was counted and is shown in the graph ($n = 5$). Anti–VLA-4 Ab treatment inhibited the increased number of vessels in the border area following CPC sheet transplantation. Lower panels show representative images. Scale bars: 100 μm. Nuclei were stained with hematoxylin. (**E**) RFP staining. The number of RFP-positive cells (brown) was counted and is shown in the graph ($n = 5$). Anti–VLA-4 Ab treatment decreased the number of RFP$^+$ cells in the infarcted area following CPC sheet transplantation. Lower panels show representative images. Nuclei were stained with hematoxylin. Scale bars: 100 μm. Data are shown as mean + SEM.

ATMCs were isolated from GFP mice as previously described (48), with a few modifications. In brief, interscapular adipose tissues were digested at 37°C in PBS, which contained 2.5 mg/ml dispase (Invitrogen), for 45 minutes. After filtration through 25-μm filters and centrifugation, isolated ATMCs were suspended in IMDM supplemented with 10% FBS and penicillin/streptomycin/amphotericin B and cultured on 1% gelatin-coated dishes. ATMCs from passages 3–5 were used for cell sheets.

Neonatal rat cardiomyocytes were isolated as previously described (19). Cardiomyocytes were plated at a field density of 1×10^5 cells/cm^2 on 24-well culture dishes (BD Falcon) coated with 1% gelatin and cultured in DMEM supplemented with 10% FBS.

Labeling of cells. Retroviral stocks were generated as previously described (19). CPCs were infected with an RFP-expressing retroviral vector. Infected cells were selected for growth in the presence of neomycin (500 μg/ml) for 2 weeks. Transfection efficiency of RFP was greater than 95%.

Direct cell injection. Within 5 minutes after ligation of the left anterior descending artery, 2.0×10^6 RFP-labeled CPCs were directly injected into the infarcted regions of wild-type mice using a Hamilton syringe.

Cell sheet preparation and transplantation. CPCs or ATMCs were suspended by trypsinization, and the cell suspension (containing 2 ml complete medium) was plated onto a 35-mm temperature-responsive dish grafted with poly(*N*-isopropylacrylamide) (PIPAAm) (Upcell; CellSeed) at 1.0×10^6 cells/dish. The cells were cultured at 37°C. After 5 days in culture, CPCs or ATMCs were incubated on temperature-responsive dishes at 20°C. After 2 hours, CPCs and ATMCs detached spontaneously and floated in the medium as monolayer cell grafts. Wild-type mice were anesthetized by an i.p. injection of 50 mg/kg sodium pentobarbital and ventilated with a volume-regulated respirator. MI was induced by ligation of the left anterior descending artery with a 10-0 Prolene suture. Mice were randomly assigned to 3 groups: mice transplanted with monolayer CPCs (CPC group; $n = 25$); mice transplanted with monolayer ATMCs (ATMC group; $n = 25$); and mice with no transplantation (MI group; $n = 25$). Within 5 minutes of coronary artery ligation, a monolayer cell sheet was placed on a plastic sheet and applied face down onto the surface of the infarcted anterior-lateral region. The plastic sheet was then carefully removed, leaving the monolayer cell sheet over the infarct area without sutures. Ten minutes after transplantation, the chest was closed.

For Ab treatment, anti–VLA-4 Abs (2.5 mg/kg) or anti-rat IgG2bκ Abs (2.5 mg/kg) as control were i.p. injected daily from 2 to 3 weeks following MI or CPC sheet transplantation.

Echocardiography and catheterization. Transthoracic echocardiography was performed with a Nemio 35 ultrasound system (Toshiba) provided with a 12-MHz imaging transducer. For catheterization analysis, the right carotid artery was cannulated under anesthesia by a micropressure transducer with an outer diameter of 0.33 mm (SPR-1000; Millar Instruments), which was then advanced into the LV. Pressure signals were recorded using a Chart5 for Windows data acquisition and analysis system (ADInstruments). Mice were anesthetized with 4% inhaled isoflurane, and the heart rate was maintained at approximately 500 bpm to minimize data deviation during cardiac function measurement.

Flow cytometric analysis. The immunostaining methods have been previously described (4). The percentage of cells expressing each cell surface antigen was analyzed with an EPICS ALTRA flow cytometer using EXPO32 software, version 1.2 (Beckman Coulter).

RNA extraction and RT-PCR. RNA extraction and RT-PCR were performed as described previously (4). Primer sequences are shown in Supplemental Table 1. Real-time PCR amplification was performed in a 7500 real-time PCR system (Applied Biosystems) using GreenER Two-Step qRT-PCR Kit Universal (Invitrogen), according to the manufacturer's instructions. The PCR protocol included an initial denaturation step (95°C, 10 minutes) followed by 50 amplification and quantification cycles (95°C for 15 seconds, 60°C for 60 seconds) and a melting curve program (60–95°C). Relative mRNA expression levels were calculated using the standard curve of pcDNA6.2-GW/EmGFP.

Western blot analysis. Whole-cell lysates (30-50 μg) were resolved by SDS-PAGE. Proteins were transferred to a PVDF membrane (GE Healthcare) and incubated with primary Abs, followed by anti-IgG horseradish peroxidase–conjugated secondary Ab. Specific proteins were detected by enhanced chemiluminescence (GE Healthcare).

Immunohistology. Hearts fixed in 4% PFA were embedded in paraffin, and 4-μm thick sections were cut and stained with Masson trichrome. The extent of fibrosis was measured in 3 sections from each heart, and the value was expressed as the ratio of Masson trichrome–stained area to total LV free wall. Vascularization was examined by measuring the number of endothelial cells in the border zone of hearts 1 and 4 weeks after MI under light microscopy. Endothelial cells were identified by immunohistochemical staining with Abs specific to vWF. Ten random microscopic fields in the border zone were examined, and the number of endothelial cells was expressed as the number of vWF-positive cells/high-power field (original magnification, ×400).

FITC-lectin perfusion assay. At 4 weeks after MI, with or without transplantation of nonlabeled CPC sheet or ATMC sheet, FITC-conjugated *Lycopersicon esculentum* (tomato) lectin (100 μl; Vector Laboratories) diluted in PBS at a concentration of 0.5 mg/ml, was injected into the tail vein of mice under anesthesia. Ten minutes after injection, the animals were perfused with 4% PFA through the LV for 5 minutes. Hearts were removed and post-fixed in 4% PFA at room temperature for 1 hour and subsequently snap-frozen in nitrogen. The fluorescent images were observed by confocal microscopy (LSM710; Zeiss) with LSM software, version 5.0 (Zeiss). Five random microscopic fields in the border zone were examined, and the number of vessels was expressed as the number of lectin-positive vessel/high-power field (original magnification, ×600).

Immunofluorescent staining. The immunostaining methods have been previously described (19). Images were taken by laser confocal microscopy (Radiance2000; Bio-Rad) or fluorescent microscopy (Zeiss) with a CCD camera (Axiocam; Zeiss).

FISH analysis. Monolayer nonlabeled CPC sheets were transplanted onto the surface of the infarcted hearts of wild-type female mice. Four weeks after transplantation, mice were sacrificed, and whole hearts were snap-frozen in nitrogen. Frozen sections were fixed with a mixture of methanol and acetic acid (3:1, v/v) for 90 minutes and subjected to FISH analysis (Cambio). The sections were air-dried and dehydrated by exposure to a graded series of ethanol solutions. They were again air-dried and incubated in 70% formamide at 65°C for 120 seconds, exposed to ice-cold 70% ethanol, and dehydrated in a graded series of ethanol solutions. Nucleotide probes were individually denatured by incubation at 65°C for 10 minutes, followed by 37°C for 60 minutes. Two (30 μl) probes were added to each slide and were hybridized overnight at 37°C. For detection of X and Y chromosomes, FITC- or Cy3-conjugated probes were used, respectively. FITC signal of FITC was amplified using an FITC amplification kit (Cambio). Nuclei were also stained with DAPI. Sections were examined by confocal microscopy (LSM710; Zeiss) and LSM software.

Cytokine Ab array and ELISA. CPCs and ATMCs (1.0×10^6) were seeded onto 10-cm dishes. After incubation for 12 hours in IMDM supplemented with 10% FBS, cells were washed with PBS thoroughly 3 times and medium was changed to serum-depleted IMDM. After incubation for 24 hours in serum-depleted medium, supernatant was collected as CM and contaminated cells were removed using a 0.45-μm filter (BD Falcon). Cytokine release was measured in culture supernatant by cytokine Ab array or ELISA, according to the manufacturer's instructions (RayBiotech Inc. and R&D Systems).

miRNA vector selection and transfection. Sense and antisense oligonucleotide primers (Supplemental Table 2) were designed in conjunction with Invitrogen. These were annealed and cloned into the pcDNA6.2-GW/EmGFP-miR vector (Invitrogen) according to the manufacturer's instructions. All constructs were sequenced to confirm correct insertion of the oligonucleotides. The pcDNA6.2-GW/EmGFP-miR-neg plasmid vector served as a negative control. Each vector was transfected to CPCs using Lipofectamine 2000 (Invitrogen) following the manufacturer's protocol. At 8 hours after transfection, the medium was exchanged. After selecting the appropriate plasmid vector by quantitative RT-PCR on VCAM-1 mRNA expression (Supplemental Figure 9B), that plasmid was transfected into CPCs and CM was collected.

Scratch-wound assay. In vitro "scratch" wounds were established by scraping cell monolayers. Cells were grown on 6-cm dishes, which were previously labeled with a traced line. After injury, the cells were gently washed several times with PBS and incubated with sVCAM-1 (10 nM) or CPC-derived CM. Cell migration from the edge of the injured monolayer was quantified by measuring the distance between wound edges at time of injury and after 24 hours incubation using an inverted phase contrast microscope (Leica) at 5 distinct positions.

Tube-like formation assay. A Matrigel tube formation assay was used to determine the effects of sVCAM-1 (10 nM) and CPC-derived CM on in vitro angiogenesis potential of HUVECs. Growth-factor reduced Matrigel (250 μl; BD Biosciences) was added to each well of a 24-well plate and allowed to polymerize at 37°C for at least 30 minutes. Trypsin-harvested HUVECs (5×10^4) were suspended in 250 μl endothelial basal medium with or without sVCAM-1 or CPC-derived CM and were seeded onto Matrigel. After incubation for 24 hours at 37°C, the cell 2D organization and the network growth area were examined using an inverted phase contrast microscope and were photographed. Tube length was quantified using LAS AF software, version 1.6.1 (Leica).

MTT assay. Neonatal rat cardiomyocytes were cultured in 24-well plates and preincubated with sVCAM-1 (100 nM) or CPC-derived CM for 24 hours in the presence or absence of anti-VLA-4 Abs (5 ng/μl), Akt inhibitor (10 μM), wortmannin (100 nM), SB203580 (10 μM), and PD98059 (10 μM). H_2O_2 (0.2 mM) was added and incubated with the cells for an additional 24 hours. After aspirating the medium, cells were washed with PBS once and 400 μl/well PBS was added. After 2 hours incubation with 5 mg/ml MTT solution, 10% SDS solution was added and incubated overnight. Supernatant OD_{570} was measured.

Apoptosis analysis. Annexin V-Cy3 Apoptosis Detection Kit (Sigma-Aldrich) was used to detect apoptotic CPCs according to the manufacturer's instructions. In brief, 2 days after miRNA plasmid vector transfection, CPCs were incubated with annexin V-Cy3 (1:100) diluted in 1× binding buffer for 5 minutes at room temperature in the dark. The number of annexin V–positive cells relative to GFP-positive cells was counted under fluorescent microscopy.

Statistics. Data are shown as mean ± SEM. Statistical analyses were performed with 2-tailed Student's *t* test for comparisons between 2 groups. Multiple group comparison was performed by 1-way ANOVA followed by Bonferroni's procedure for comparison of means. $P < 0.05$ was considered significant.

Acknowledgments

We thank R. Kobayashi, A. Furuyama, H. Nagao, and K. Yoshihara for their excellent technical assistance. We thank M. Okabe, Osaka University, for the GFP transgenic mice and Shunichi Morikawa, Tokyo Women's Medical University, for his technical advice. This study was supported by a grant-in-aid for Scientific Research on Priority Areas and for Exploratory Research, Ministry of Education, Culture, Sports, Science and Technology: Health (to I. Komuro); the Cell Science Research Foundation and the Takeda Science Foundation (to T. Nagai); Health and Labour Sciences Research grants (to T. Shimizu); a grant-in-aid for Scientific Research, Developmental Scientific Research, and Scientific Research from the Ministry of Education, Science, Sports, and Culture; the Sakakibara Memorial Foundation; the Hisako Yamakawa Award and a Japan Heart Foundation/Novartis Grant for Research Award on Molecular and Cellular Cardiology, 2009, Takeda Science Foundation (to K. Matsuura).

Received for publication September 15, 2008, and accepted in revised form May 27, 2009.

Address correspondence to: Katsuhisa Matsuura, Department of Cardiology, Tokyo Women's Medical University, 8-1 Kawadacho, Shinjuku-ku, Tokyo, 162-8666, Japan. Phone: 81-3-3353-8111; Fax: 81-3-3356-0441; E-mail: mkatu2002@yahoo.co.jp. Or to: Issei Komuro, Department of Cardiovascular Science and Medicine, Chiba University Graduate School of Medicine, 1-8-1 Inohana, Chuo-ku, Chiba 260-8670, Japan. Phone: 81-43-226-2097; Fax: 81-43-226-2096; E-mail: komuro-tky@umin.ac.jp.

1. Dimmeler, S., Zeiher, A.M., and Schneider, M.D. 2005. Unchain my heart: the scientific foundations of cardiac repair. *J. Clin. Invest.* **115**:572–583.
2. Beltrami, A.P., et al. 2003. Adult cardiac stem cells are multipotent and support myocardial regeneration. *Cell.* **114**:763–776.
3. Oh, H., et al. 2003. Cardiac progenitor cells from adult myocardium: homing, differentiation, and fusion after infarction. *Proc. Natl. Acad. Sci. U. S. A.* **100**:12313–12318.
4. Matsuura, K., et al. 2004. Adult cardiac Sca-1-positive cells differentiate into beating cardiomyocytes. *J. Biol. Chem.* **279**:11384–11391.
5. Messina, E., et al. 2004. Isolation and expansion of adult cardiac stem cells from human and murine heart. *Circ. Res.* **95**:911–921.
6. Laugwitz, K.L., et al. 2005. Postnatal isl1+ cardioblasts enter fully differentiated cardiomyocyte lineages. *Nature.* **433**:647–653.
7. Smith, R.R., et al. 2007. Regenerative potential of cardiosphere-derived cells expanded from percutaneous endomyocardial biopsy specimens. *Circulation.* **115**:896–908.
8. Mirotsou, M., et al. 2007. Secreted frizzled related protein 2 (Sfrp2) is the key Akt-mesenchymal stem cell-released paracrine factor mediating myocardial survival and repair. *Proc. Natl. Acad. Sci. U. S. A.* **104**:1643–1648.
9. Cho, H.J., et al. 2007. Role of host tissues for sustained humoral effects after endothelial progenitor cell transplantation into the ischemic heart. *J. Exp. Med.* **204**:3257–3269.
10. Schächinger, V., et al. 2006. Intracoronary bone marrow-derived progenitor cells in acute myocardial infarction. *N. Engl. J. Med.* **355**:1210–1221.
11. Perin, E.C., et al. 2008. Comparison of intracoronary and transendocardial delivery of allogeneic mesenchymal cells in a canine model of acute myocardial infarction. *J. Mol. Cell. Cardiol.* **44**:486–495.
12. Beeres, S.L., et al. 2007. Intramyocardial injection of autologous bone marrow mononuclear cells in patients with chronic myocardial infarction and severe left ventricular dysfunction. *Am. J. Cardiol.* **100**:1094–1098.
13. Zhang, M., et al. 2001. Cardiomyocyte grafting for cardiac repair: graft cell death and anti-death strategies. *J. Mol. Cell. Cardiol.* **33**:907–921.
14. Okano, T., et al. 1993. A novel recovery system for cultured cells using plasma-treated polystyrene dishes grafted with poly (N-isopropylacrylamide). *J. Biomed. Mater. Res.* **27**:1243–1251.
15. Kushida, A., et al. 1999. Decrease in culture temperature releases monolayer endothelial cell sheets together with deposited fibronectin matrix from temperature-responsive culture surfaces. *J. Biomed. Mater. Res.* **45**:355–362.
16. Memon, I.A., et al. 2005. Repair of impaired myocardium by means of implantation of engineered autologous myoblast sheets. *J. Thorac. Cardiovasc. Surg.* **130**:1333–1341.
17. Miyahara, Y., et al. 2006. Monolayered mesenchymal stem cells repair scarred myocardium after myocardial infarction. *Nat. Med.* **12**:459–465.
18. Hida, N., et al. 2008. Novel cardiac precursor-like cells from human menstrual blood-derived mesenchymal cells. *Stem Cells.* **26**:1695–1704.
19. Matsuura, K., et al. 2004. Cardiomyocytes fuse with surrounding noncardiomyocytes and reenter the cell cycle. *J. Cell. Biol.* **167**:351–363.
20. Limana, F., et al. 2002. bcl-2 overexpression promotes myocyte proliferation. *Proc. Natl. Acad. Sci. U. S. A.* **99**:6257–6262.
21. Giancotti, F.G., and Ruoslahti, E. 1999. Integrin signaling. *Science.* **285**:1028–1032.
22. Nakao, S., Kuwano, T., Ishibashi, T., Kuwano, M., and Ono, M. 2003. Synergistic effect of TNF-alpha in soluble VCAM-1-induced angiogenesis through alpha 4 integrins. *J. Immunol.* **170**:5704–5711.
23. Funk, P.E., Stephan, R.P., and Witte, P.L. 1995. Vascular cell adhesion molecule 1-positive reticular cells express interleukin-7 and stem cell factor in the bone marrow. *Blood.* **86**:2661–2671.
24. Garton, K.J., et al. 2003. Stimulated shedding of vascular cell adhesion molecule 1 (VCAM-1) is mediated by tumor necrosis factor-alpha-converting enzyme (ADAM 17). *J. Biol. Chem.* **278**:37459–37464.
25. Satoh, M., et al. 1999. Tumor necrosis factor-α-converting enzyme and tumor necrosis factor-α in human dilated cardiomyopathy. *Circulation.* **99**:3260–3265.
26. Shi, W., et al. 2003. TACE is required for fetal murine cardiac development and modeling. *Dev. Biol.* **261**:371–380.
27. Koch, A.E., Halloran, M.M., Haskell, C.J., Shah, M.R., and Polverini, P.J. 1995. Angiogenesis mediated by soluble forms of E-selectin and vascular cell adhesion molecule-1. *Nature.* **376**:517–519.
28. Chan, B.M., Elices, M.J., Murphy, E., Hemler, M.E. 1992. Adhesion to vascular cell adhesion molecule 1 and fibronectin. Comparison of alpha 4beta 1 (VLA-4) and alpha 4 beta 7 on the human B cell line JY. *J. Biol. Chem.* **267**:8366–8370.
29. Shai, S.Y., et al. 2002. Cardiac myocyte-specific excision of the beta1 integrin gene results in myocardial fibrosis and cardiac failure. *Circ. Res.* **90**:458–464.
30. Watt, F.M. 2002. Role of integrins in regulating epidermal adhesion, growth and differentiation. *EMBO J.* **21**:3919–3926.
31. Papayannopoulou, T. 2003. Bone marrow homing: the players, the playfield, and their evolving roles. *Curr. Opin. Hematol.* **10**:214–219.
32. Muraski, J.A., et al. 2007. Pim-1 regulates cardiomyocyte survival downstream of Akt. *Nat. Med.* **13**:1467–1475.
33. Purcell, N.H., et al. 2007. Genetic inhibition of cardiac ERK1/2 promotes stress-induced apop-

tosis and heart failure but has no effect on hypertrophy in vivo. *Proc. Natl. Acad. Sci. U. S. A.* **104**:14074–14079.
34. Kwee, L., et al. 1995. Defective development of the embryonic and extraembryonic circulatory systems in vascular cell adhesion molecule (VCAM-1) deficient mice. *Development.* **121**:489–503.
35. Yang, J.T., Rayburn, H., and Hynes, R.O. 1995. Cell adhesion events mediated by alpha 4 integrins are essential in placental and cardiac development. *Development.* **121**:549–560.
36. Urbanek, K., et al. 2006. Stem cell niches in the adult mouse heart. *Proc. Natl. Acad. Sci. U. S. A.* **103**:9226–9231.
37. Hsieh, P.C., et al. 2007. Evidence from a genetic fate-mapping study that stem cells refresh adult mammalian cardiomyocytes after injury. *Nat. Med.* **13**:970–974.
38. Tousoulis, D., et al. 2007. Differences in inflammatory and thrombotic markers between unstable angina and acute myocardial infarction. *Int. J. Cardiol.* **115**:203–207.
39. Zhang, S., et al. 2007. Fusion of human hematopoietic progenitor cells and murine cardiomyocytes is mediated by alpha 4 beta 1 integrin/vascular cell adhesion molecule-1 interaction. *Circ. Res.* **100**:693–702.
40. Wang, X., et al. 2006. The role of the sca-1+/CD31- cardiac progenitor cell population in postinfarction left ventricular remodeling. *Stem Cells.* **24**:1779–1788.
41. Kogata, N., et al. 2006. Cardiac ischemia activates vascular endothelial cadherin promoter in both preexisting vascular cells and bone marrow cells involved in neovascularization. *Circ. Res.* **98**:897–904.
42. Elmadbouh, I., et al. 2007. Ex vivo delivered stromal cell-derived factor-1alpha promotes stem cell homing and induces angiomyogenesis in the infarcted myocardium. *J. Mol. Cell. Cardiol.* **42**:792–803.
43. Qin, G., et al. 2006. Functional disruption of alpha4 integrin mobilizes bone marrow-derived endothelial progenitors and augments ischemic neovascularization. *J. Exp. Med.* **203**:153–163.
44. Urbanek, K., et al. 2005. Cardiac stem cells possess growth factor-receptor systems that after activation regenerate the infarcted myocardium, improving ventricular function and long-term survival. *Circ. Res.* **97**:663–673.
45. Zhu, W., et al. 2008. IGFBP-4 is an inhibitor of canonical Wnt signalling required for cardiogenesis. *Nature.* **454**:345–349.
46. Shimizu, T., et al. 2006. Polysurgery of cell sheet grafts overcomes diffusion limits to produce thick, vascularized myocardial tissues. *FASEB J.* **20**:708–710.
47. Bock-Marquette, I., Saxena, A., White, M.D., Dimaio, J.M., and Srivastava, D. 2004. Thymosin beta4 activates integrin-linked kinase and promotes cardiac cell migration, survival and cardiac repair. *Nature.* **432**:466–472.
48. Planat-Bénard, V., et al. 2004. Spontaneous cardiomyocyte differentiation from adipose tissue stroma cells. *Circ. Res.* **94**:223–229.

Cardiac 12/15 lipoxygenase–induced inflammation is involved in heart failure

Yosuke Kayama,[1,4] Tohru Minamino,[1,2] Haruhiro Toko,[1] Masaya Sakamoto,[3] Ippei Shimizu,[1] Hidehisa Takahashi,[1] Sho Okada,[1] Kaoru Tateno,[1] Junji Moriya,[1] Masataka Yokoyama,[1] Aika Nojima,[1] Michihiro Yoshimura,[4] Kensuke Egashira,[5] Hiroyuki Aburatani,[6] and Issei Komuro[1]

[1]Department of Cardiovascular Science and Medicine, Chiba University Graduate School of Medicine, Chuo-ku, Chiba 260-8670, Japan
[2]PRESTO, Japan Science and Technology Agency, Saitama 332-0012, Japan
[3]Department of Diabetes, Metabolism and Endocrinology and [4]Department of Cardiology, Jikei University School of Medicine, Minato-ku, Tokyo 105-8461, Japan
[5]Department of Cardiovascular Medicine, Graduate School of Medical Sciences, Kyushu University, Higashi-ku, Fukuoka 812-8582, Japan
[6]Genome Science Division, Research Center for Advanced Science and Technology, University of Tokyo, Meguro-ku, Tokyo 153-8904, Japan

To identify a novel target for the treatment of heart failure, we examined gene expression in the failing heart. Among the genes analyzed, *Alox15* encoding the protein 12/15 lipoxygenase (LOX) was markedly up-regulated in heart failure. To determine whether increased expression of 12/15-LOX causes heart failure, we established transgenic mice that overexpressed 12/15-LOX in cardiomyocytes. Echocardiography showed that *Alox15* transgenic mice developed systolic dysfunction. Cardiac fibrosis increased in *Alox15* transgenic mice with advancing age and was associated with the infiltration of macrophages. Consistent with these observations, cardiac expression of monocyte chemoattractant protein 1 (MCP-1) was up-regulated in *Alox15* transgenic mice compared with wild-type mice. Treatment with 12-hydroxy-eicosatetraenoic acid, a major metabolite of 12/15-LOX, increased MCP-1 expression in cardiac fibroblasts and endothelial cells but not in cardiomyocytes. Inhibition of MCP-1 reduced the infiltration of macrophages into the myocardium and prevented both systolic dysfunction and cardiac fibrosis in *Alox15* transgenic mice. Likewise, disruption of 12/15-LOX significantly reduced cardiac MCP-1 expression and macrophage infiltration, thereby improving systolic dysfunction induced by chronic pressure overload. Our results suggest that cardiac 12/15-LOX is involved in the development of heart failure and that inhibition of 12/15-LOX could be a novel treatment for this condition.

CORRESPONDENCE
Issei Komuro:
komuro-tky@umin.ac.jp

Abbreviations used: cDNA, complementary DNA; FS, fractional shortening; HETE, hydroxy-eicosatetraenoic acids; LOX, lipoxygenase; LVDd, left ventricular diastolic dimension; MCP-1, monocyte chemoattractant protein 1; mRNA, messenger RNA; TAC, transverse aortic constriction.

Heart failure is a clinical syndrome that is associated with various cardiovascular diseases such as hypertension and myocardial infarction (Libby and Braunwald, 2008). Comprehensive management using current therapeutic options can markedly reduce the morbidity and mortality of heart failure. Large-scale clinical trials of drugs targeting neurohormonal mechanisms, such as angiotensin-converting enzyme inhibitors and β blockers, have shown that such treatment is effective for reducing mortality in patients with heart failure (Garg and Yusuf, 1995; McMurray, 1999; Goldstein, 2002). However, heart failure is still one of the leading causes of death worldwide (Libby and Braunwald, 2008), so it is important to investigate the underlying mechanisms of this condition and develop more effective treatments.

Arachidonic acid is a free fatty acid that, when liberated from cell membranes, can be metabolized by cyclooxygenase, cytochrome p450, and lipoxygenase (LOX) to form biologically active products such as prostaglandins, leukotrienes, and hydroxy-eicosatetraenoic acids (HETEs;

Y. Kayama, T. Minamino, and H. Toko contributed equally to this paper.

The Rockefeller University Press $30.00
J. Exp. Med. Vol. 206 No. 7 1565–1574
www.jem.org/cgi/doi/10.1084/jem.20082596

Kudo and Murakami, 2002). LOXs are a family of lipid-peroxidizing enzymes that oxidize free and esterified polyenolic fatty acids to form the corresponding hydroperoxy derivates (Kuhn and O'Donnell, 2006). The LOX enzymes are named according to the specific carbon atoms of arachidonic acid that are oxidized. Thus, 12/15-LOX is a member of the LOX family that catalyzes the step from arachidonic acid to 12(S)-HETE and 15(S)-HETE (Chen et al., 1994). 12/15-LOX was originally isolated from porcine leukocytes (Yokoyama et al., 1986), but its tissue distribution is now known to be relatively wide, including blood vessels, the brain, and the kidneys (Kuhn and O'Donnell, 2006). Several lines of evidence have suggested that 12/15-LOX may play an important role in the development of atherosclerosis, diabetes, and neurodegenerative disease (Natarajan and Nadler, 2004; Kuhn and O'Donnell, 2006). For example, disruption of the gene for 12/15-LOX in mice significantly reduces the onset of atherosclerosis (Cyrus et al., 1999, 2001; George et al., 2001), whereas an increase of 12/15-LOX expression in mice promotes monocyte–endothelial cell interactions that lead to atherogenesis (Hatley et al., 2003; Reilly et al., 2004; Bolick et al., 2005). Several studies have shown that monocyte 12/15-LOX mediates the oxidative modification of low-density lipoprotein (McNally et al., 1990; Sakashita et al., 1999; Zhu et al., 2003b). An increase of 12/15-LOX activity in vessel walls also contributes to atherogenesis by impairing the macrophage cholesterol efflux pathway (Nagelin et al., 2008). Interestingly, mice with deficiency of 12/15-LOX are resistant to the development of streptozotocin-induced diabetes (Bleich et al., 1999) and autoimmune diabetes (McDuffie et al., 2008). However, there is currently little evidence that 12/15-LOX has a role in heart failure.

In the present study, we showed that cardiac 12/15-LOX induces inflammation that is involved in heart failure. We found that 12/15-LOX expression was markedly increased in the failing heart. Increased expression of this enzyme up-regulates monocyte chemoattractant protein 1 (MCP-1) and promotes the infiltration of macrophages into the heart, thereby causing cardiac fibrosis and systolic dysfunction. Conversely, disruption of *Alox15* reduces cardiac MCP-1 expression and macrophage infiltration, thereby improving systolic dysfunction induced by chronic pressure overload. These findings suggest that inhibition of 12/15-LOX could be a novel treatment for heart failure.

RESULTS

Increased expression of 12/15-LOX causes heart failure

To clarify the molecular mechanisms of heart failure, we performed microarray analysis using cardiac tissue samples obtained from a hypertensive heart failure model (Dahl salt-sensitive rats). Approximately 300 genes showed significant changes of expression in failing hearts compared with control hearts. For example, fetal genes, such as the natriuretic peptide genes and the β-type myosin heavy chain gene, were up-regulated, whereas cardioprotective genes, such as heat shock proteins, were down-regulated (Table S1). Among the genes analyzed, *Alox15* encoding the protein 12/15-LOX was most markedly up-regulated in failing hearts compared with control hearts (Fig. 1 A). Northern blot analysis confirmed that the messenger RNA (mRNA) for this gene was strikingly elevated in heart failure (Fig. 1 B). Immunohistochemistry showed that expression of 12/15-LOX was specifically up-regulated in cardiomyocytes of failing hearts (Fig. 1 C).

To determine whether increased expression of 12/15-LOX could cause heart failure, we established *Alox15* transgenic mice in which expression of the murine *Alox15* gene was under the control of the α-cardiac myosin heavy chain promoter. We obtained two lines of transgenic mice, both of which showed an ~10-fold increase in the myocardial expression of 12/15-LOX compared with their WT littermates (Fig. 2 A; and Fig. S1, A and B). Histological examination also indicated that the transgenic mice showed increased myocardial expression of 12/15-LOX (Fig. 2 B and Fig. S1 C). Consequently, production of 12(S)-HETE and 15(S)-HETE was significantly increased in the hearts of *Alox15* transgenic mice (Fig. 2 C). The left ventricular diastolic dimension (LVDd) was increased and left ventricular fractional shortening (FS) was decreased in *Alox15* transgenic mice from 26 wk of age compared with their WT littermates (Fig. 2 D). These changes observed in the transgenic animals showed further progression with aging (Fig. 2 D). Histological examination revealed that cardiac fibrosis was increased in *Alox15* transgenic mice and that this fibrosis also progressed with advancing age and was associated with infiltration of macrophages (Fig. 2, E and F). There was no difference in blood pressure between *Alox15* transgenic mice and their WT littermates at 16 or 48 wk of age (Fig. S1 D). The cardiac changes were similar in two independent lines of *Alox15* transgenic mice, suggesting that increased expression of 12/15-LOX might cause heart failure by inducing myocardial inflammation.

12/15-LOX induces cardiac inflammation

To investigate the mechanism by which cardiac infiltration of macrophages was increased in *Alox15* transgenic mice, we examined the expression of various proinflammatory cytokines that are thought to be macrophage chemoattractants by the ribonuclease protection assay. We found that cardiac expression of *Ccl2* (MCP-1) was significantly increased in *Alox15* transgenic mice compared with WT mice (Fig. 3 A). In vitro experiments demonstrated that treatment with 12(S)-HETE increased *Ccl2* expression by cardiac fibroblasts and endothelial cells (Fig. 3, B and C), whereas there was no effect when cardiomyocytes were treated with 12(S)-HETE (Fig. 3 D). Moreover, incubation of COS7 cells with 12(S)-HETE significantly increased the activity of nuclear factor κB, a transcription factor that regulates the induction of proinflammatory cytokines including MCP-1 (Fig. 3 E). In contrast, 12(S)-HETE did not affect the activity of this factor when cells were transfected with a reporter plasmid containing mutant κB binding sites (Fig. 3 E). These results suggest that increased production of 12(S)-HETE by cardiomyocytes

causes up-regulation of MCP-1 in other cells of the heart, thereby leading to accumulation of macrophages.

To investigate the relationship between up-regulation of MCP-1 and heart failure, we examined the effect of MCP-1 inhibition on cardiac dysfunction in *Alox15* transgenic mice. We injected an expression vector encoding mutant human MCP-1 with deletion of N-terminal amino acids (7ND plasmid; Egashira, 2003) or the empty vector (mock) into the thigh muscles of mice every 2 wk until 48 wk of age. The result was a significant increase in the blood level of 7ND and elevation of plasma human MCP-1 (Fig. 4 A and Fig. S2). This mutant MCP-1 binds to the MCP-1 receptor (chemokine receptor 2) and inhibits downstream signaling (Egashira, 2003). Consequently, injection of the 7ND plasmid has been reported to suppress MCP-1 activity in vivo and inhibit the development of atherosclerosis (Ni et al., 2001), as well as inhibiting cardiac remodelling after myocardial infarction (Hayashidani et al., 2003). In agreement with these results,

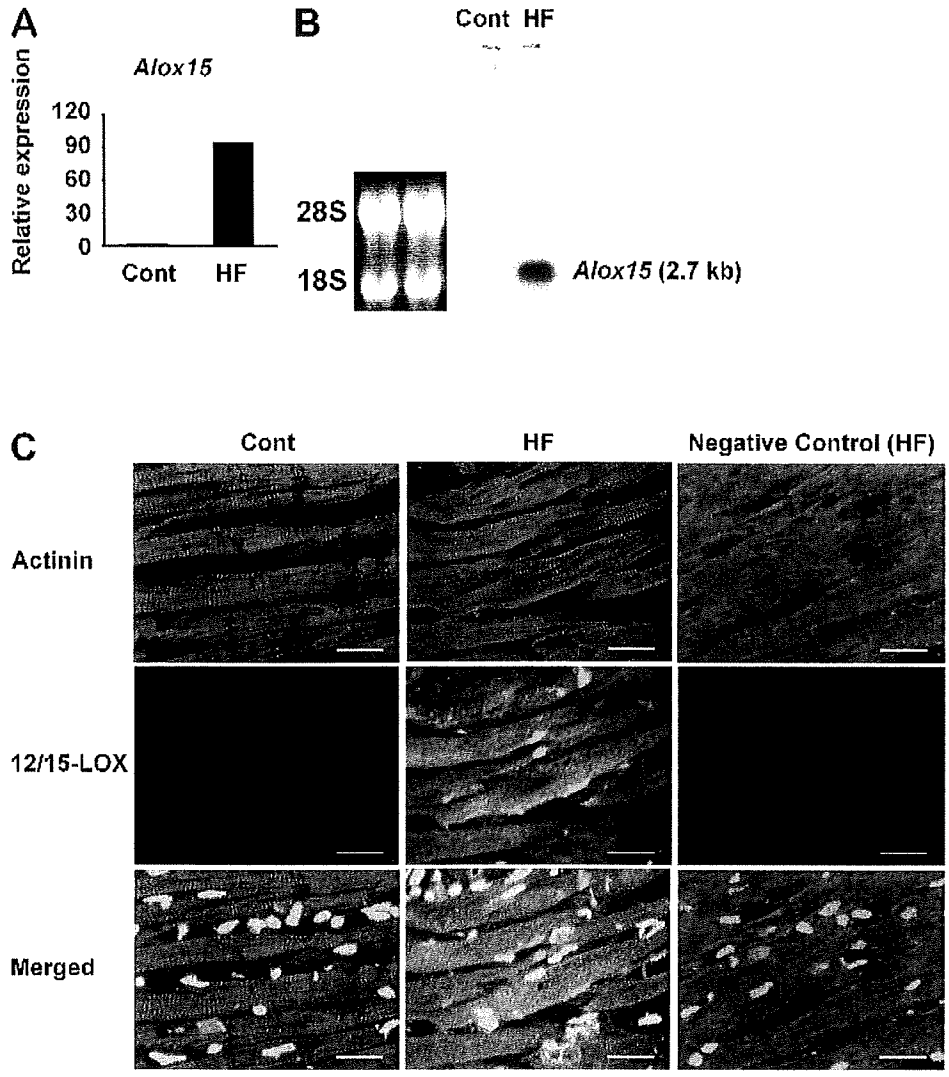

Figure 1. Expression of 12/15-LOX is up-regulated in the failing heart. (A) Dahl salt-sensitive rats were fed a low-sodium diet until the age of 6 wk and then a high-sodium diet (8% NaCl) throughout the experimental period. In this model, prominent cardiac hypertrophy developed and left ventricular systolic function was impaired by 17 wk of age. Rats fed a low-salt diet (0.3% NaCl) served as the control. The animals were sacrificed for gene chip analysis at 17 wk of age. Expression of *Alox15* was markedly up-regulated in failing hearts (HF) compared with control hearts (Cont). (B) Northern blot analysis confirmed that the expression of mRNA for *Alox15* was strikingly elevated in failing hearts. (C) Immunohistochemistry for 12/15-LOX in the heart at 17 wk of age. Expression of 12/15-LOX (red) was specifically up-regulated in cardiomyocytes (green) of failing hearts. Nuclei were stained with DAPI (blue). Bars, 20 µm. Normal rabbit serum was used as a negative control of polyclonal antibody against 12/15-LOX. Results in A are obtained from one experiment. Results in B and C are representative of three independent experiments.

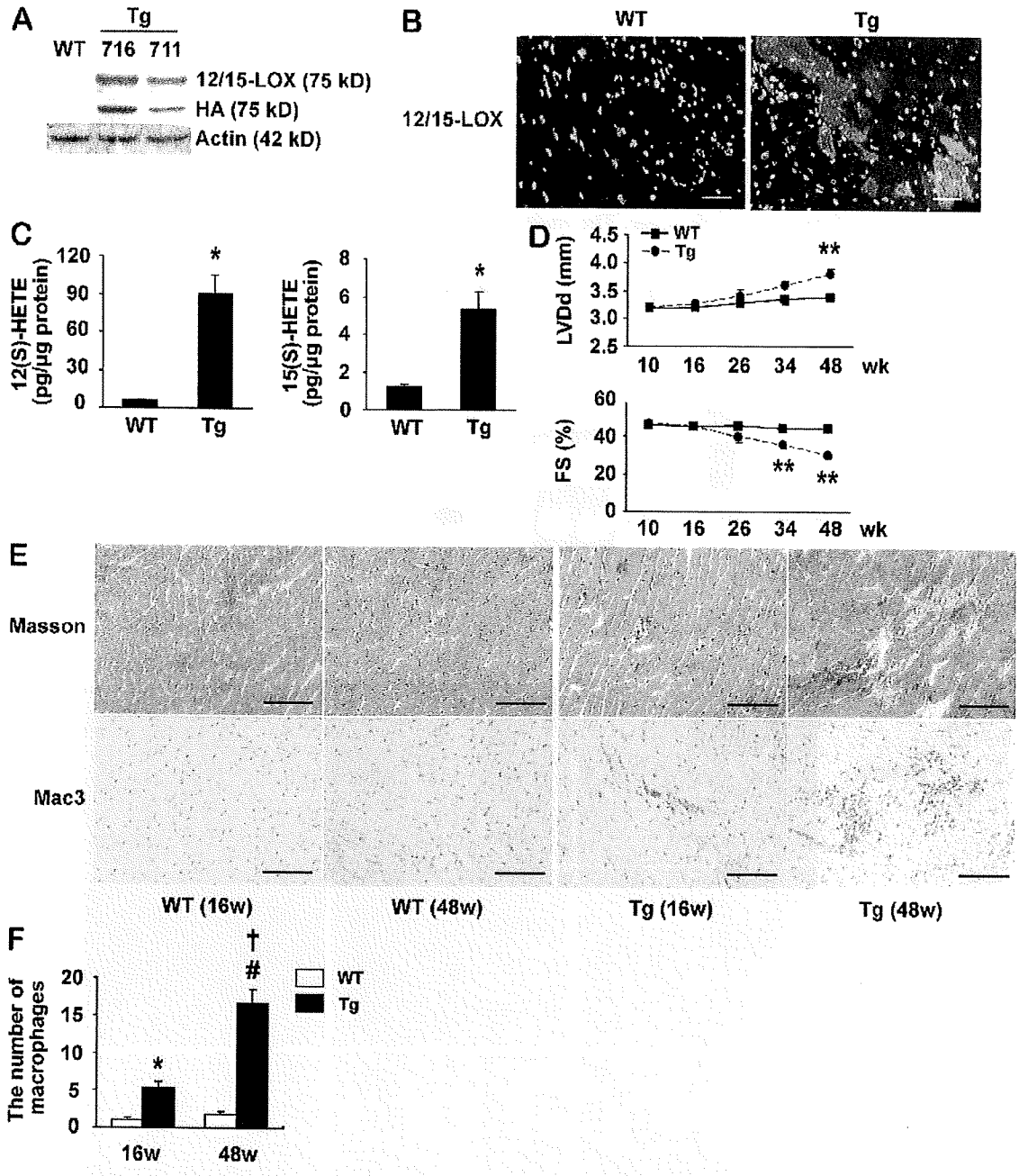

Figure 2. Increased expression of 12/15-LOX causes heart failure. (A) Western blot analysis of 12/15-LOX expression in the hearts of WT and *Alox15* transgenic (Tg) mice using anti-12/15-LOX antibody (12/15-LOX) or anti-HA antibody (HA). (B) Immunohistochemistry for 12/15-LOX (red) in the hearts of WT and *Alox15* transgenic mice. Nuclei were stained with DAPI (blue). Bars, 40 μm. Results in A and B are representative of three independent experiments. (C) 12/15(S)-HETE levels in the hearts of WT and *Alox15* transgenic mice. (D) Echocardiographic findings in WT and transgenic mice. The LVDd was increased and left ventricular FS was decreased in *Alox15* transgenic mice compared with their WT littermates. These changes observed in the transgenic animals showed progression with aging. *, $P < 0.05$; **, $P < 0.01$ versus WT. Results in C and D represent the mean ± SEM of three independent experiments. C, $n = 6$; D, $n = 14$. (E) Masson trichrome staining (top) and immunohistochemistry for Mac3 (bottom) in the hearts of WT and transgenic mice at the ages of 16 wk (16w) and 48 wk (48w). Cardiac fibrosis was increased in *Alox15* transgenic mice, and this fibrosis progressed with advancing age and was associated with infiltration of macrophages. Bars, 100 μm. Results are representative of three independent experiments. (F) The number of Mac3-positive cells in the hearts of WT and transgenic mice at the ages of 16 wk (16w) and 48 wk (48w). *, $P < 0.01$ versus WT (16w); #, $P < 0.01$ versus WT (48w); †, $P < 0.01$ versus transgenic (16w). Results represent the mean ± SEM of three independent experiments; $n = 7$.

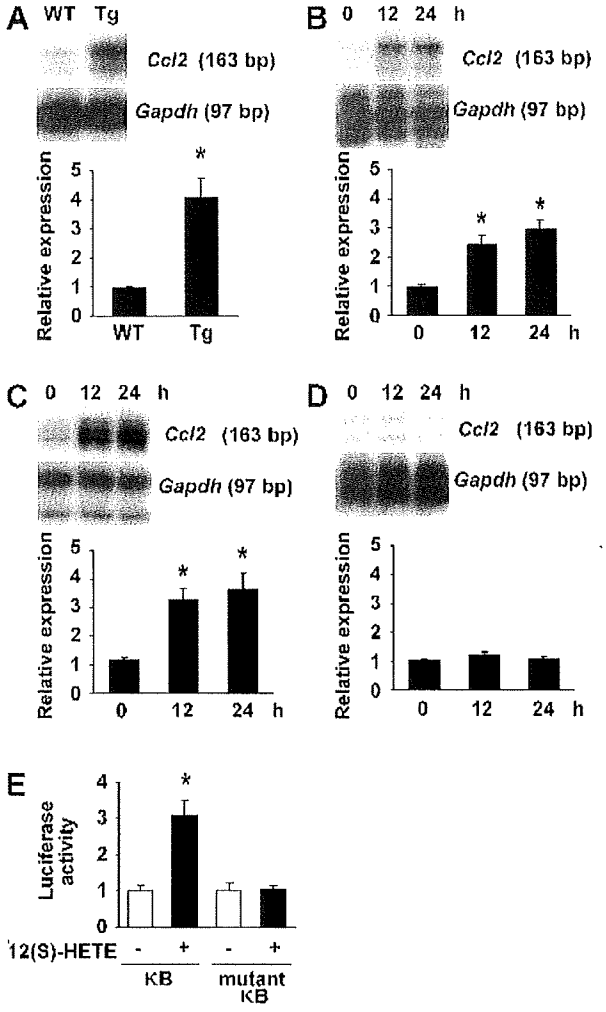

Figure 3. 12/15-LOX up-regulates MCP-1 expression. (A) Expression of *Ccl2* (MCP-1) was examined in the hearts of WT and *12/15-LOX* transgenic (Tg) mice by the ribonuclease protection assay. The graph indicates relative expression of *Ccl2*. Cardiac expression of *Ccl2* was significantly greater in *Alox15* transgenic mice than in WT mice. *, $P < 0.05$ versus WT. Results represent the mean ± SEM of three independent experiments; $n = 6$. (B–D) Cardiac fibroblasts (B), endothelial cells (C), and cardiomyocytes (D) were treated with 5×10^{-7} M 12(S)-HETE for the indicated times (0–24 h), and expression of *Ccl2* was examined by the ribonuclease protection assay. Graphs display relative expression of *Ccl2*. Incubation with 12(S)-HETE increased *Ccl2* expression by cardiac fibroblasts and endothelial cells. *, $P < 0.01$ versus time 0. Results represent mean ± SEM of four independent experiments; $n = 4$ for B and C; $n = 7$ for D. (E) The luciferase reporter gene plasmid containing the κB binding site was transfected into COS7 cells, which were cultured in the absence or presence of 5×10^{-7} M 12(S)-HETE. The luciferase assay was performed 12 h later. A reporter plasmid containing the mutant κB binding site was used as the negative control. Incubation of cells with 12(S)-HETE significantly increased the activity of nuclear factor κB. *, $P < 0.01$ versus 12(S)-HETE (−)/κB. Results represent the mean ± SEM of five independent experiments; $n = 6$.

histological examination and echocardiography demonstrated that injection of this plasmid reduced the myocardial infiltration of macrophages in *Alox15* transgenic mice, as well as preventing systolic dysfunction and left ventricular dilatation (Fig. 4, B and C). These results suggested that 12/15-LOX induces cardiac dysfunction by up-regulation of MCP-1 expression in the heart.

Cardiac expression of 12/15-LOX is up-regulated during pressure overload

To further investigate the role of 12/15-LOX in heart failure, we examined its cardiac expression in WT mice with severe transverse aortic constriction (TAC). In this model, cardiac hypertrophy gradually progresses to reach a peak on day 7 after TAC and then decreases afterward (not depicted). FS was preserved until day 7 but was significantly decreased on day 14 along with left ventricular dilatation (Fig. 5 A). Cardiac expression of *Alox15* was significantly up-regulated after TAC (Fig. 5 B), and the production of both 12(S)-HETE and 15(S)-HETE was increased in the heart (Fig. 5 C). Histological examination demonstrated an increase in the expression of 12/15-LOX by cardiomyocytes after TAC (Fig. 6 A and Fig. S3).

We next created *Alox15*-deficient mice with TAC and compared them to WT TAC mice. The increase of 12(S)-HETE and 15(S)-HETE production after TAC was markedly attenuated by disruption of *Alox15* (Fig. 6). Disruption of *Alox15* also significantly improved systolic dysfunction and prevented left ventricular dilatation in the presence of chronic pressure overload without any change of blood pressure (Fig. 5 A and Fig. S4), indicating that 12/15-LOX has an important role in the induction of cardiac dysfunction by pressure overload. To examine whether *Alox15* deficiency could inhibit cardiac inflammation, we assessed the expression of *Ccl2* and a macrophage marker (Cd68) in the heart after TAC. Expression of both genes was increased by about threefold at 14 d after TAC. The increase of *Ccl2* and *Cd68* expression was significantly inhibited by disruption of *Alox15* (Fig. 6 C), suggesting that this gene has a crucial role in the development of heart failure by promoting cardiac inflammation.

DISCUSSION

We demonstrated a crucial role of 12/15-LOX–induced inflammation in the development of heart failure. Activation of this enzyme has been shown to promote neuronal death, whereas inhibition of 12/15-LOX protects against brain damage caused by oxidative stress or ischemia by inhibiting neuronal death (Lebeau et al., 2004; Jin et al., 2008; Seiler et al., 2008). In contrast, treatment with 12(S)-HETE does not induce the apoptosis of cultured cardiomyocytes (unpublished data). Indeed, few apoptotic cardiomyocytes were detected in the hearts of *Alox15* transgenic mice even after the onset of systolic dysfunction (unpublished data). Instead, these mice showed an increase of macrophages infiltrating into the myocardium, which was associated with cardiac fibrosis and systolic dysfunction. Our findings suggested that MCP-1 may

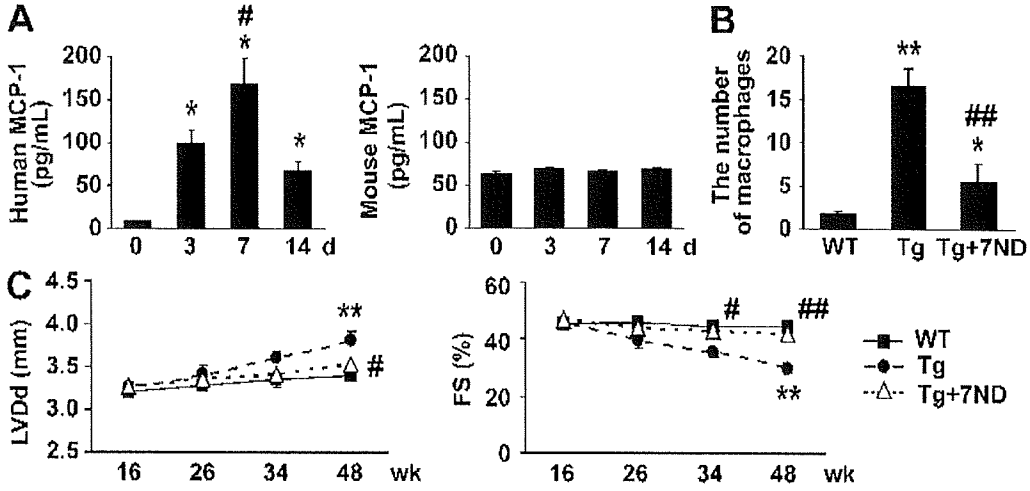

Figure 4. Inhibition of MCP-1 prevents cardiac dysfunction in *Alox15* transgenic animals. (A) The plasma levels of 7ND (human MCP-1) and murine MCP-1 were determined by ELISA at the indicated times after introduction of the 7ND expression vector. The plasma level of human MCP-1 was significantly increased after injection of the 7ND plasmid. *, $P < 0.01$ versus day 0; #, $P < 0.01$ versus day 3. Results represent the mean ± SEM of three independent experiments; $n = 5$. (B) Number of Mac3-positive cells in the hearts of WT mice, transgenic (Tg) mice, and transgenic mice treated with 7ND (Tg + 7ND). Injection of the 7ND plasmid reduced the myocardial infiltration of macrophages in *Alox15* transgenic mice. (C) Echocardiographic findings in WT mice, transgenic mice, and transgenic mice treated with 7ND (Tg + 7ND). Injection of the 7ND plasmid prevented systolic dysfunction and left ventricular dilatation in *Alox15* transgenic mice. *, $P < 0.05$; **, $P < 0.01$ versus WT; #, $P < 0.05$; ##, $P < 0.01$ versus transgenic. Results represent mean ± SEM of three independent experiments. B, $n = 7$; C, $n = 10$–14.

have a major role in promoting cardiac inflammation in *Alox15* transgenic mice because its inhibition almost completely abolished the accumulation of macrophages and prevented systolic dysfunction. We also showed that 12/15-LOX induces up-regulation of MCP-1 expression in the setting of pressure overload, thereby increasing cardiac inflammation and leading to systolic dysfunction. Consistent with our findings, inhibition of MCP-1 has been reported to attenuate

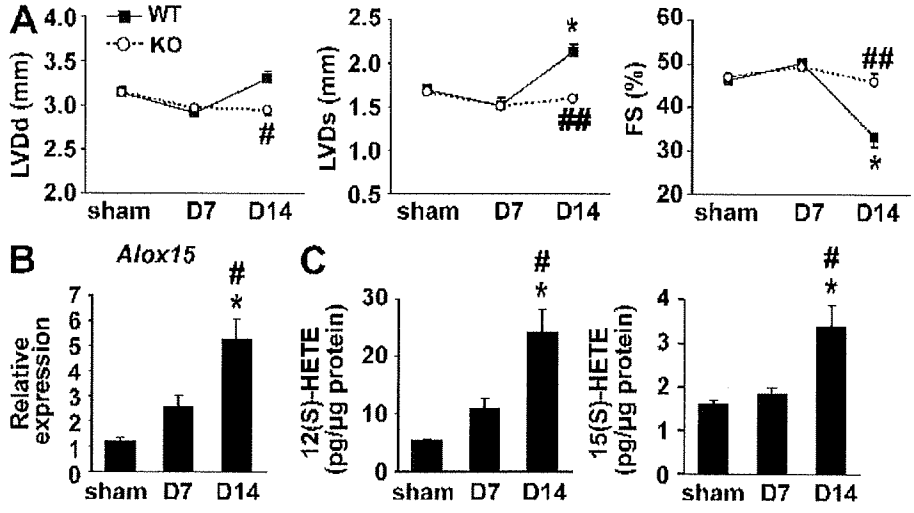

Figure 5. Cardiac expression of 12/15-LOX is up-regulated during pressure overload. (A) Echocardiographic findings in WT and *Alox15*-deficient (KO) mice on day 7 (D7) and day 14 (D14) after TAC surgery. FS was preserved until day 7 but was significantly decreased on day 14 along with left ventricular dilatation in WT mice. Disruption of *Alox15* (KO) significantly improved systolic dysfunction and prevented left ventricular dilatation caused by chronic pressure overload. LVDs, left ventricular systolic dimension; sham, sham operation. *, $P < 0.01$ versus sham; #, $P < 0.05$; ##, $P < 0.01$ versus WT. Results represent the mean ± SEM of three independent experiments; $n = 10$. (B and C) *Alox15* expression (B) and the 12/15(S)-HETE level (C) were examined in the hearts of WT mice on day 7 (D7) and day 14 (D14) after TAC surgery by real-time PCR and ELISA, respectively. Cardiac expression of 12/15-LOX was significantly up-regulated after TAC, and production of both 12(S)-HETE and 15(S)-HETE was increased in the heart. *, $P < 0.01$ versus sham; #, $P < 0.01$ versus D7. Results represent the mean ± SEM of three independent experiments; $n = 6$.

myocardial inflammation, fibrosis, and cardiac dysfunction induced by chronic pressure overload (Kuwahara et al., 2004). It has also been reported that transgenic animals with cardiac expression of MCP-1 develop myocardial fibrosis and systolic dysfunction (Kolattukudy et al., 1998). In agreement with our in vitro data, it has been reported that MCP-1 expression is up-regulated in vascular endothelial cells and fibroblasts by pressure overload (Kuwahara et al., 2004). Collectively, these

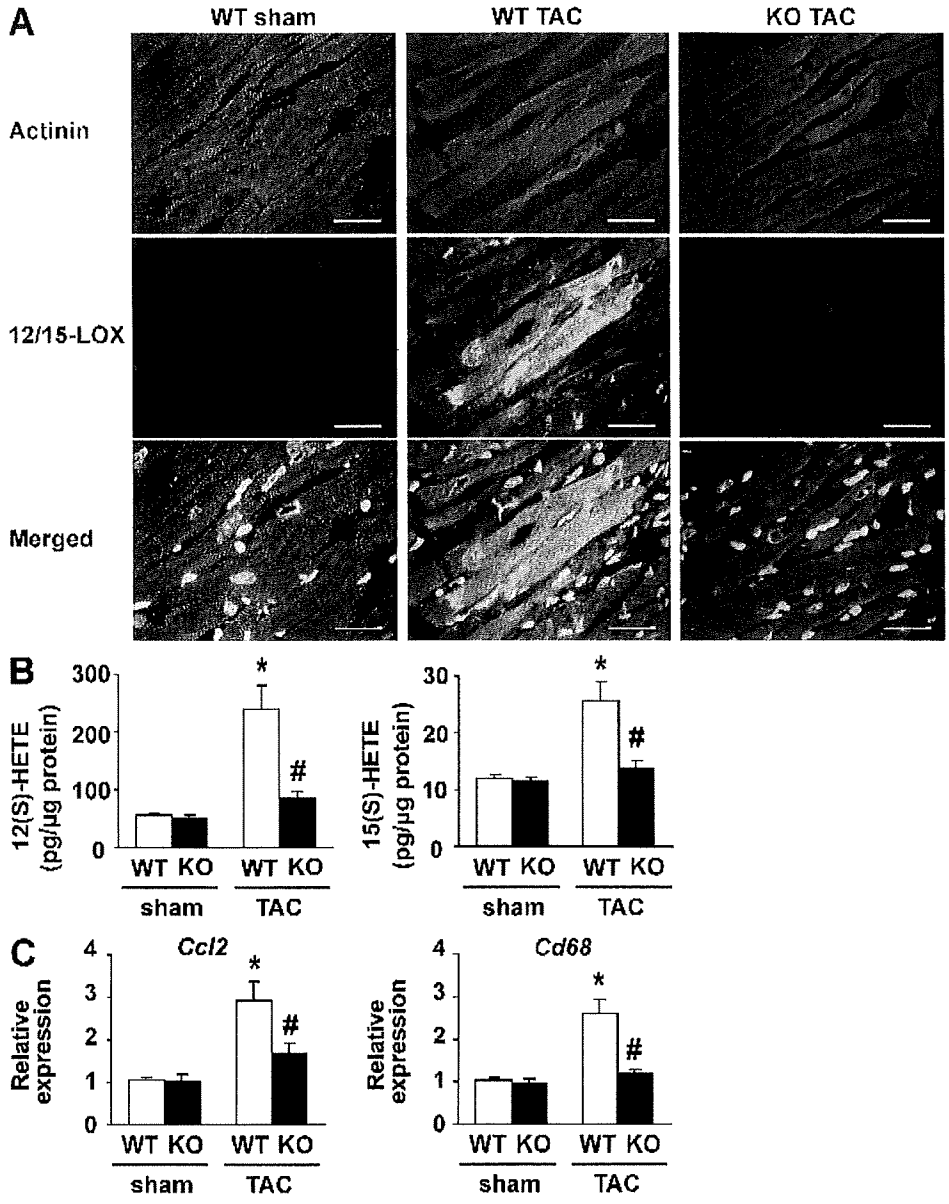

Figure 6. Disruption of *Alox15* attenuates cardiac inflammation during pressure overload. (A) Double immunostaining for 12/15-LOX (red) and actinin (green) in the hearts of sham-operated WT mice (WT sham), WT mice with TAC (WT TAC), and *Alox15*-deficient mice with TAC (KO TAC). Increased expression of 12/15-LOX was observed in cardiomyocytes after TAC in WT mice but not KO mice. Nuclei were stained with DAPI (blue). Bars, 20 μm. Results are representative of four independent experiments. (B) 12/15(S)-HETE levels were examined in the hearts of WT and *Alox15*-deficient (KO) mice after sham surgery or TAC. The increase of 12(S)-HETE and 15(S)-HETE production after TAC was markedly attenuated in *Alox15*-deficient mice (KO). *, $P < 0.01$ versus WT sham; #, $P < 0.01$ versus WT TAC. Results represent the mean ± SEM of three independent experiments; $n = 6–8$. (C) Expression of *Ccl2* (MCP-1) and *Cd68* was examined in the hearts of WT and *Alox15*-deficient (KO) mice after sham surgery or TAC. Expression of both genes was increased by about threefold at 14 d after TAC. This increase of expression was significantly inhibited by disruption of *Alox15*. *, $P < 0.01$ versus WT sham; #, $P < 0.01$ versus WT TAC. Results represent the mean ± SEM of three independent experiments; $n = 6–8$.

results indicate that chronic pressure overload increases the expression of 12/15-LOX, which then causes heart failure by promoting cardiac inflammation and fibrosis.

Target gene disruption or overexpression of 12/15-LOX in mice with a genetic background of apolipoprotein E or low-density lipoprotein receptor deficiency has shown that this enzyme may have a role in atherogenesis. The data indirectly support a role for 12/15-LOX in the oxidative modification of low-density lipoprotein. Consistent with our results, recent evidence suggests that 12/15-LOX plays a crucial role in the regulation of proinflammatory molecules and that this regulatory activity of 12/15-LOX may be important for linking 12/15-LOX activation to atherogenesis. For example, 12(S)-HETE increases the expression of MCP-1, interleukin 6, tumor necrosis factor α, and adhesion molecules by macrophages and vascular cells (Bolick et al., 2005, 2006; Wen et al., 2007, 2008; Dwarakanath et al., 2008), and these changes are partly mediated by activation of nuclear factor κB (Bolick et al., 2005, 2006; Dwarakanath et al., 2008). Disruption of 12/15-LOX has also been shown to attenuate airway allergic inflammation by modulating the expression of proinflammatory cytokines (Andersson et al., 2008).

The mechanism of 12/15-LOX activation in the failing heart is unclear. We previously demonstrated that mismatch between the number of capillaries and the size of cardiomyocytes occurs during the development of cardiac hypertrophy, leading to myocardial hypoxia and systolic dysfunction (Sano et al., 2007). Because exposure of cultured cardiomyocytes to hypoxia up-regulates 12/15-LOX expression (unpublished data), a hypoxic state might be one reason for the induction of 12/15-LOX in the failing heart. This concept is supported by previous results that hypoxia up-regulates 12/15-LOX expression in the lungs and the brain (Bernaudin et al., 2002; Zhu et al., 2003a). Moreover, we have found that 12/15-LOX expression is significantly up-regulated in the heart after myocardial infarction (unpublished data). There are putative binding elements for CCAAT/enhancer binding proteins and nuclear factor κB within the promoter region of the *Alox15* gene (unpublished data), and both of these molecules are known to be activated by hypoxia (Cummins and Taylor, 2005).

Inflammation has an important role in the pathogenesis and progression of many forms of heart failure, and biomarkers of inflammation have become the subject of intense investigation. In the Framingham Heart Study, an increase of C-reactive protein (as well as inflammatory cytokines such as interleukin 6 and tumor necrosis factor α) was found to identify asymptomatic older persons in the community with a high risk of developing heart failure in the future (Braunwald, 2008). Multivariate analysis has shown that an increase of C-reactive protein is an independent predictor of adverse outcomes in patients with acute or chronic heart failure (Anand et al., 2005), suggesting that heart failure is closely associated with systemic inflammation. Because metabolites of 12/15-LOX may have a role in vascular inflammation, insulin resistance, and renal dysfunction (Natarajan and Nadler, 2004; Kuhn and O'Donnell, 2006), activation of 12/15-LOX in the failing heart could induce systemic inflammation and have a detrimental effect on other inflammatory diseases such as atherosclerosis, metabolic syndrome, and nephropathy. Conversely, inhibition of 12/15-LOX could be an attractive new strategy for the treatment of heart failure, as well as various other inflammatory conditions.

MATERIALS AND METHODS

Animal models. All of the experimental protocols were approved by Chiba University review board. Male Dahl salt-sensitive (DS) rats were purchased from SLC. The rats were fed a low-sodium diet until the age of 6 wk and then a high-sodium diet (8% NaCl) throughout the experimental period. In this model, marked cardiac hypertrophy developed and left ventricular systolic function was impaired at 17 wk of age. Accordingly, DS rats were sacrificed for gene chip analysis at 17 wk. All of the DS rats given a high-sodium diet showed signs of heart failure such as rapid and labored respiration and diffuse left ventricular hypokinesis on echocardiography at the time of sacrifice. Other DS rats were fed a low-salt diet (0.3% NaCl) as a control group.

We generated transgenic mice on a C57BL/6 background that expressed 12/15-LOX in cardiomyocytes under the control of the α-cardiac myosin heavy chain (α-MHC) promoter. A mouse *Alox15* complementary DNA (cDNA) fragment (gift from C.D. Funk, University of Pennsylvania, Philadelphia, PA) fused with the HA tag was subcloned into the α-MHC promoter vector. The transgene was identified by genomic PCR with transgene-specific oligonucleotide primers (5′-CCACACCAGAAATGACAGAC-3′ and 5′-GCGGGCAGGGAGACAAGTAG-3′) and by Southern blot analysis. Two independent lines of *Alox15* transgenic mice (lines 711 and 716) were obtained. The cardiac phenotype was similar in both lines of transgenic animals. WT littermates were used as the control for all experiments.

Alox15-deficient mice on a C57BL/6 background were purchased from The Jackson Laboratory. WT littermates served as a control for all experiments. TAC was performed as described previously (Sano et al., 2007) on 10–11-wk-old male mice. Sham-operated mice underwent the same procedure without aorta constriction.

An expression vector encoding mutant human MCP-1 with deletion of N-terminal amino acids (7ND plasmid) was prepared as described elsewhere (Hayashidani et al., 2003). Under anesthesia, mice received an injection of 100 μg of either the empty vector or the 7ND plasmid in PBS into the bilateral tibial muscles using a 27-gauge needle fitted with a plastic collar that limited muscle penetration to ~5 mm. Injection was performed every 2 wk from 10 wk until 48 wk of age. To increase the efficiency of gene transfection, 100 μl of the myotoxic agent bupivacaine (0.25% wt/vol) was injected into the muscles 3 d before transfection. Transfection of 7ND leads to an increase of mutant MCP-1 in the blood, as indicated by elevation of its plasma concentration after 14 d. The circulating mutant MCP-1 binds to the receptor for MCP-1 (chemokine receptor 2) on target cells and effectively blocks MCP-1 signaling (Ni et al., 2001; Hayashidani et al., 2003).

Physiological and histological analysis. Echocardiography was performed with a Vevo 770 High Resolution Imaging System (Visual Sonics Inc.). To minimize variation of the data, the heart rate was ~500–600 beats per minute when cardiac function was assessed. The peak systolic blood pressure was recorded by a photoelectric pulse devise (Blood Pressure Meter BP-98A; Softron Co. Ltd.) placed on the tails of unanesthetized mice. Under anesthesia, a micropressure transducer with an outer diameter of 0.42 mm (Samba 201 control unit and Samba Preclin 420 transducer; Samba Sensors AB) was introduced into the right carotid artery. Pressure signals were recorded with a MacLab 3.6/s data acquisition system (AD Instruments) at a sampling rate of 2,000 Hz. 4-μm frozen cross sections of the heart were fixed in 4% paraformaldehyde and subjected to Masson trichrome staining or immunohistochemistry for Mac3 (BD). Digital photographs were taken at 400× magnification of 25 random fields from each heart, and the number of Mac3-positive cells was counted in each field. The frozen cardiac cross sections

were also stained with antibodies for 12/15-LOX (Cayman Chemical) and actinin (Sigma-Aldrich).

DNA chip analysis. 10 μg of total RNA was extracted from the left ventricles of rats by the Li-Urea method and was used to synthesize biotin-labeled cRNA, which was then hybridized to a high-density oligonucleotide array (Gene Chip U34A array; Affymetrix) according to the previously published protocol (Ishii et al., 2000). The array contains probe sets for ~8,800 genes and ESTs, which were selected from Build 34 of the UniGene Database (created from GenBank 107/dbEST 11/18/98). GeneChip 3.3 software (Affymetrix) was used to calculate the mean difference for each probe on the array, which showed the intensity of gene expression defined by Affymetrix using their algorithm. The mean difference has been shown to quantitatively reflect the abundance of a particular mRNA in a population. The data were deposited in GEO (GSM406556, GSM406557, and GSE16199).

RNA analysis. Total RNA was isolated from the hearts of mice with RNAZol-B (Molecular Research Center, Cincinnati, OH) and the ribonuclease protection assay (RiboQuant; BD) was performed according to the manufacturer's instructions. For Northern blot analysis, 30 μg of total RNA was separated on formaldehyde denaturing gel and transferred to a nylon membrane (GE Healthcare). Then the blot was hybridized with radiolabeled *Alox15* cDNA probe using Quickhyb hybridization solution (Agilent Technologies) according to the manufacturer's instructions. Rat *Alox15* cDNA fragment was a gift from T. Yoshimoto (Kanazawa University Graduate School of Medical Science, Kanazawa, Japan). Mouse *Alox12* cDNA fragment was a gift from C.D. Funk. Real-time PCR was performed using a LightCycler (Roche) with the Taqman Universal Probe Library and the Light Cycler Master (Roche) according to the manufacturer's instructions.

Western blot analysis. Whole cell lysates were prepared in lysis buffer (10 mM Tris-HCl, pH 8, 140 mM NaCl, 5 mM EDTA, 0.025% NaN_3, 1% Triton X-100, 1% deoxycholate, 0.1% SDS, 1 mM PMSF, 5 μg/ml leupeptin, 2 μg/ml aprotinin, 50 mM NaF, and 1 mM $Na2VO_3$). 40–50 μg of the lysates were resolved by SDS-PAGE (PAGE). Then proteins were transferred to a nitrocellulose membrane (GE Healthcare), which was incubated with the primary antibody, followed by anti–rabbit or anti–mouse immunoglobulin G conjugated with horseradish peroxidase (Jackson ImmunoResearch Laboratories). Specific proteins were detected by using enhanced chemiluminescence (GE Healthcare). The primary antibodies used for Western blotting were as follows: anti-HA antibody (Santa Cruz Biotechnology, Inc.), anti–12/15-LOX antibody (Cayman Chemical), and anti-actin antibody (Sigma-Aldrich). ELISA was performed according to the manufacturer's instructions to examine the levels of 12(S)-HETE, 15(S)-HETE (Assay Designs), human MCP-1, and mouse MCP-1 (Invitrogen).

Cell culture. Neonatal Wistar rats were purchased from Takasugi Experimental Animal Supply. Cardiomyocytes and cardiac fibroblasts were prepared from these neonatal rats and cultured as described previously (Sano et al., 2007). Human umbilical vein endothelial cells (BioWhittaker; Lonza) were cultured according to the manufacturer's instructions.

Luciferase assay. 1 μg of the reporter gene plasmid was transfected into COS7 cells at 24 h before the luciferase assay. 0.1 μg of the control vector encoding *Renilla* luciferase was cotransfected as an internal control. The assay was performed using a dual luciferase reporter assay system (Promega) according to the manufacturer's instructions. p55-A2-Luc (the luciferase reporter gene containing the κB binding site) was a gift from T. Fujita (The Tokyo Metropolitan Institute of Medical Science, Tokyo, Japan; Fujita et al., 1993).

Statistical analysis. Data are shown as the mean ± SEM. Multiple group comparison was performed by one-way ANOVA, followed by Bonferroni's test for comparison of means. Comparisons between two groups were done with the two-tailed unpaired Student's *t* test or two-way ANOVA. In all analyses, $P < 0.05$ was considered statistically significant.

Online supplemental material. Fig. S1 depicts *Alox15* transgenic animal data. Fig. S2 shows MCP-1 levels after treatment with 7ND. Fig. S3 shows a negative control of immunohistochemistry for 12/15-LOX. Fig. S4 shows blood pressure of *Alox15*-deficient mice. Table S1 summarizes the microarray data. Online supplemental material is available at http://www.jem.org/cgi/content/full/jem.20082596/DC1.

We thank Dr. C. Funk, Dr. T. Yoshimoto, and Dr. T. Fujita for reagents and E. Fujita, R. Kobayashi, Y. Ishiyama, and M. Ikeda for technical support.

This work was supported by a Grant-in-Aid for Scientific Research from the Ministry of Education, Science, Sports, and Culture, and Health and Labor Sciences Research Grants (to I. Komuro), a Grant-in-Aid for Scientific Research from the Ministry of Education, Culture, Sports, Science and Technology of Japan, grants from the Suzuken Memorial Foundation, the Japan Diabetes Foundation, the Ichiro Kanehara Foundation, the Tokyo Biochemical Research Foundation, and the Cell Science Research Foundation (to T. Minamino), grants from the Takeda Science Foundation and the Japan Foundation of Applied Enzymology (to T. Minamino and H. Toko), and Sakakibara Memorial research Grant from the Japan Research Promotion Society for Cardiovascular Disease (to H. Toko).

The authors declare no competing financial interests.

Submitted: 17 November 2008
Accepted: 29 May 2009

REFERENCES

Anand, I.S., R. Latini, V.G. Florea, M.A. Kuskowski, T. Rector, S. Masson, S. Signorini, P. Mocarelli, A. Hester, R. Glazer, and J.N. Cohn. 2005. C-reactive protein in heart failure: prognostic value and the effect of valsartan. *Circulation.* 112:1428–1434.

Andersson, C.K., H.E. Claesson, K. Rydell-Tormanen, S. Swedmark, A. Hallgren, and J.S. Erjefalt. 2008. Mice lacking 12/15-lipoxygenase have attenuated airway allergic inflammation and remodeling. *Am. J. Respir. Cell Mol. Biol.* 39:648–656.

Bernaudin, M., Y. Tang, M. Reilly, E. Petit, and F.R. Sharp. 2002. Brain genomic response following hypoxia and re-oxygenation in the neonatal rat. Identification of genes that might contribute to hypoxia-induced ischemic tolerance. *J. Biol. Chem.* 277:39728–39738.

Bleich, D., S. Chen, B. Zipser, D. Sun, C.D. Funk, and J.L. Nadler. 1999. Resistance to type 1 diabetes induction in 12-lipoxygenase knockout mice. *J. Clin. Invest.* 103:1431–1436.

Bolick, D.T., A.W. Orr, A. Whetzel, S. Srinivasan, M.E. Hatley, M.A. Schwartz, and C.C. Hedrick. 2005. 12/15-lipoxygenase regulates intercellular adhesion molecule-1 expression and monocyte adhesion to endothelium through activation of RhoA and nuclear factor-kappaB. *Arterioscler. Thromb. Vasc. Biol.* 25:2301–2307.

Bolick, D.T., S. Srinivasan, A. Whetzel, L.C. Fuller, and C.C. Hedrick. 2006. 12/15 lipoxygenase mediates monocyte adhesion to aortic endothelium in apolipoprotein E-deficient mice through activation of RhoA and NF-kappaB. *Arterioscler. Thromb. Vasc. Biol.* 26:1260–1266.

Braunwald, E. 2008. Biomarkers in heart failure. *N. Engl. J. Med.* 358:2148–2159.

Chen, X.S., U. Kurre, N.A. Jenkins, N.G. Copeland, and C.D. Funk. 1994. cDNA cloning, expression, mutagenesis of C-terminal isoleucine, genomic structure, and chromosomal localizations of murine 12-lipoxygenases. *J. Biol. Chem.* 269:13979–13987.

Cummins, E.P., and C.T. Taylor. 2005. Hypoxia-responsive transcription factors. *Pflugers Arch.* 450:363–371.

Cyrus, T., J.L. Witztum, D.J. Rader, R. Tangirala, S. Fazio, M.F. Linton, and C.D. Funk. 1999. Disruption of the 12/15-lipoxygenase gene diminishes atherosclerosis in apo E-deficient mice. *J. Clin. Invest.* 103:1597–1604.

Cyrus, T., D. Pratico, L. Zhao, J.L. Witztum, D.J. Rader, J. Rokach, G.A. FitzGerald, and C.D. Funk. 2001. Absence of 12/15-lipoxygenase expression decreases lipid peroxidation and atherogenesis in apolipoprotein e-deficient mice. *Circulation.* 103:2277–2282.

Dwarakanath, R.S., S. Sahar, L. Lanting, N. Wang, M.B. Stemerman, R. Natarajan, and M.A. Reddy. 2008. Viral vector-mediated

12/15-lipoxygenase overexpression in vascular smooth muscle cells enhances inflammatory gene expression and migration. *J. Vasc. Res.* 45:132–142.

Egashira, K. 2003. Molecular mechanisms mediating inflammation in vascular disease: special reference to monocyte chemoattractant protein-1. *Hypertension.* 41:834–841.

Fujita, T., G.P. Nolan, H.C. Liou, M.L. Scott, and D. Baltimore. 1993. The candidate proto-oncogene bcl-3 encodes a transcriptional coactivator that activates through NF-kappa B p50 homodimers. *Genes Dev.* 7:1354–1363.

Garg, R., and S. Yusuf. 1995. Overview of randomized trials of angiotensin-converting enzyme inhibitors on mortality and morbidity in patients with heart failure. Collaborative group on ACE inhibitor trials. *JAMA.* 273:1450–1456.

George, J., A. Afek, A. Shaish, H. Levkovitz, N. Bloom, T. Cyrus, L. Zhao, C.D. Funk, E. Sigal, and D. Harats. 2001. 12/15-Lipoxygenase gene disruption attenuates atherogenesis in LDL receptor-deficient mice. *Circulation.* 104:1646–1650.

Goldstein, S. 2002. Benefits of beta-blocker therapy for heart failure: weighing the evidence. *Arch. Intern. Med.* 162:641–648.

Hatley, M.E., S. Srinivasan, K.B. Reilly, D.T. Bolick, and C.C. Hedrick. 2003. Increased production of 12/15 lipoxygenase eicosanoids accelerates monocyte/endothelial interactions in diabetic db/db mice. *J. Biol. Chem.* 278:25369–25375.

Hayashidani, S., H. Tsutsui, T. Shiomi, M. Ikeuchi, H. Matsusaka, N. Suematsu, J. Wen, K. Egashira, and A. Takeshita. 2003. Anti-monocyte chemoattractant protein-1 gene therapy attenuates left ventricular remodeling and failure after experimental myocardial infarction. *Circulation.* 108:2134–2140.

Ishii, M., S. Hashimoto, S. Tsutsumi, Y. Wada, K. Matsushima, T. Kodama, and H. Aburatani. 2000. Direct comparison of GeneChip and SAGE on the quantitative accuracy in transcript profiling analysis. *Genomics.* 68:136–143.

Jin, G., K. Arai, Y. Murata, S. Wang, M.F. Stins, E.H. Lo, and K. van Leyen. 2008. Protecting against cerebrovascular injury: contributions of 12/15-lipoxygenase to edema formation after transient focal ischemia. *Stroke.* 39:2538–2543.

Kolattukudy, P.E., T. Quach, S. Bergese, S. Breckenridge, J. Hensley, R. Altschuld, G. Gordillo, S. Klenotic, C. Orosz, and J. Parker-Thornburg. 1998. Myocarditis induced by targeted expression of the MCP-1 gene in murine cardiac muscle. *Am. J. Pathol.* 152:101–111.

Kudo, I., and M. Murakami. 2002. Phospholipase A2 enzymes. *Prostaglandins Other Lipid Mediat.* 68–69:3–58.

Kuhn, H., and V.B. O'Donnell. 2006. Inflammation and immune regulation by 12/15-lipoxygenases. *Prog. Lipid Res.* 45:334–356.

Kuwahara, F., H. Kai, K. Tokuda, M. Takeya, A. Takeshita, K. Egashira, and T. Imaizumi. 2004. Hypertensive myocardial fibrosis and diastolic dysfunction: another model of inflammation? *Hypertension.* 43:739–745.

Lebeau, A., F. Terro, W. Rostene, and D. Pelaprat. 2004. Blockade of 12-lipoxygenase expression protects cortical neurons from apoptosis induced by beta-amyloid peptide. *Cell Death Differ.* 11:875–884.

Libby, P., and E. Braunwald. 2008. Braunwald's Heart Disease: a Textbook of Cardiovascular Medicine. Saunders/Elsevier, Philadelphia. 509 pp.

McDuffie, M., N.A. Maybee, S.R. Keller, B.K. Stevens, J.C. Garmey, M.A. Morris, E. Kropf, C. Rival, K. Ma, J.D. Carter, et al. 2008. Nonobese diabetic (NOD) mice congenic for a targeted deletion of 12/15-lipoxygenase are protected from autoimmune diabetes. *Diabetes.* 57:199–208.

McMurray, J.J. 1999. Major beta blocker mortality trials in chronic heart failure: a critical review. *Heart.* 82:IV14–IV22.

McNally, A.K., G.M. Chisolm III, D.W. Morel, and M.K. Cathcart. 1990. Activated human monocytes oxidize low-density lipoprotein by a lipoxygenase-dependent pathway. *J. Immunol.* 145:254–259.

Nagelin, M.H., S. Srinivasan, J. Lee, J.L. Nadler, and C.C. Hedrick. 2008. 12/15-Lipoxygenase activity increases the degradation of macrophage ATP-binding cassette transporter G1. *Arterioscler. Thromb. Vasc. Biol.* 28:1811–1819.

Natarajan, R., and J.L. Nadler. 2004. Lipid inflammatory mediators in diabetic vascular disease. *Arterioscler. Thromb. Vasc. Biol.* 24:1542–1548.

Ni, W., K. Egashira, S. Kitamoto, C. Kataoka, M. Koyanagi, S. Inoue, K. Imaizumi, C. Akiyama, K.I. Nishida, and A. Takeshita. 2001. New anti-monocyte chemoattractant protein-1 gene therapy attenuates atherosclerosis in apolipoprotein E-knockout mice. *Circulation.* 103:2096–2101.

Reilly, K.B., S. Srinivasan, M.E. Hatley, M.K. Patricia, J. Lannigan, D.T. Bolick, G. Vandenhoff, H. Pei, R. Natarajan, J.L. Nadler, and C.C. Hedrick. 2004. 12/15-Lipoxygenase activity mediates inflammatory monocyte/endothelial interactions and atherosclerosis in vivo. *J. Biol. Chem.* 279:9440–9450.

Sakashita, T., Y. Takahashi, T. Kinoshita, and T. Yoshimoto. 1999. Essential involvement of 12-lipoxygenase in regiospecific and stereospecific oxidation of low density lipoprotein by macrophages. *Eur. J. Biochem.* 265:825–831.

Sano, M., T. Minamino, H. Toko, H. Miyauchi, M. Orimo, Y. Qin, H. Akazawa, K. Tateno, Y. Kayama, M. Harada, et al. 2007. p53-induced inhibition of Hif-1 causes cardiac dysfunction during pressure overload. *Nature.* 446:444–448.

Seiler, A., M. Schneider, H. Forster, S. Roth, E.K. Wirth, C. Culmsee, N. Plesnila, E. Kremmer, O. Radmark, W. Wurst, et al. 2008. Glutathione peroxidase 4 senses and translates oxidative stress into 12/15-lipoxygenase dependent- and AIF-mediated cell death. *Cell Metab.* 8:237–248.

Wen, Y., J. Gu, S.K. Chakrabarti, K. Aylor, J. Marshall, Y. Takahashi, T. Yoshimoto, and J.L. Nadler. 2007. The role of 12/15-lipoxygenase in the expression of interleukin-6 and tumor necrosis factor-alpha in macrophages. *Endocrinology.* 148:1313–1322.

Wen, Y., J. Gu, G.E. Vandenhoff, X. Liu, and J.L. Nadler. 2008. Role of 12/15-lipoxygenase in the expression of MCP-1 in mouse macrophages. *Am. J. Physiol. Heart Circ. Physiol.* 294:H1933–H1938.

Yokoyama, C., F. Shinjo, T. Yoshimoto, S. Yamamoto, J.A. Oates, and A.R. Brash. 1986. Arachidonate 12-lipoxygenase purified from porcine leukocytes by immunoaffinity chromatography and its reactivity with hydroperoxyeicosatetraenoic acids. *J. Biol. Chem.* 261:16714–16721.

Zhu, D., M. Medhora, W.B. Campbell, N. Spitzbarth, J.E. Baker, and E.R. Jacobs. 2003a. Chronic hypoxia activates lung 15-lipoxygenase, which catalyzes production of 15-HETE and enhances constriction in neonatal rabbit pulmonary arteries. *Circ. Res.* 92:992–1000.

Zhu, H., Y. Takahashi, W. Xu, H. Kawajiri, T. Murakami, M. Yamamoto, S. Iseki, T. Iwasaki, H. Hattori, and T. Yoshimoto. 2003b. Low density lipoprotein receptor-related protein-mediated membrane translocation of 12/15-lipoxygenase is required for oxidation of low density lipoprotein by macrophages. *J. Biol. Chem.* 278:13350–13355.